Cell Reports

Article

Aedes aegypti sialokinin facilitates mosquito blood feeding and modulates host immunity and vascular biology

Graphical abstract

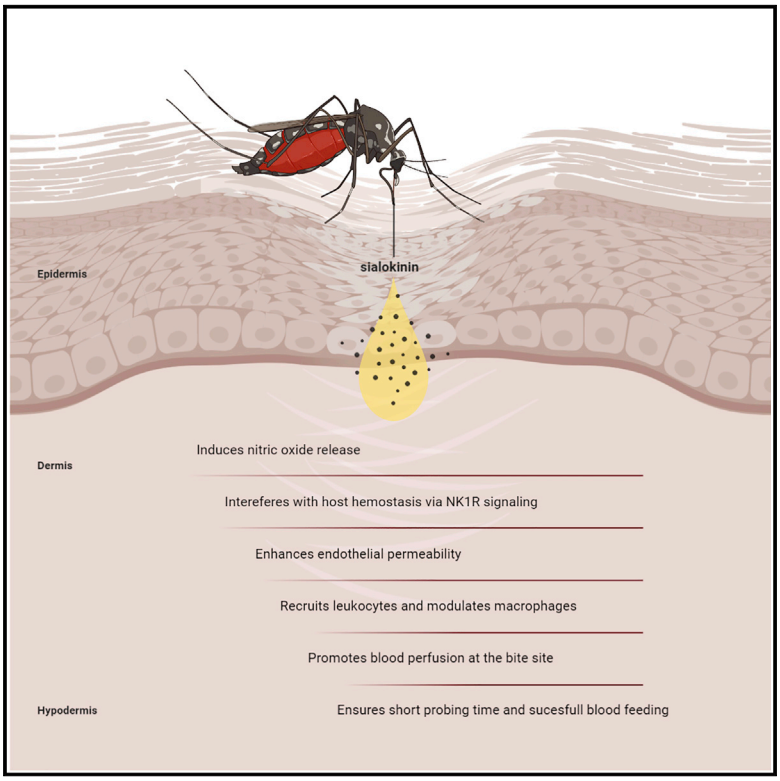

Highlights

- The vasodilator sialokinin induces nitric oxide release similarly to substance P
- Sialokinin KO mosquitoes shows lower blood perfusion and longer probing time
- Sialokinin interferes with host hemostasis via NK1R signaling
- Sialokinin promotes endothelial permeability and leukocyte recruitment

Authors

Ines Martin-Martin, Paola Carolina Valenzuela Leon, Laura Amo, ..., Hans Ackerman, Zach N. Adelman, Eric Calvo

Correspondence

martinines@hotmail.com (I.M.-M.), ecalvo@niaid.nih.gov (E.C.)

In brief

Martin-Martin et al. describe the function of an *Aedes aegypti* salivary peptide, sialokinin. It modulates macrophages, alters endothelial permeability, promotes leukocyte recruitment, induces nitric oxide release, and interferes with hemostasis via NK1R signaling. Sialokinin promotes blood perfusion and ensures short probing time. These findings demonstrate its antihemostatic and immunomodulator role.

Martin-Martin et al., 2022, Cell Reports *39*, 110648
April 12, 2022
https://doi.org/10.1016/j.celrep.2022.110648

CellPress

Cell Reports

CellPress
OPEN ACCESS

Article

Aedes aegypti sialokinin facilitates mosquito blood feeding and modulates host immunity and vascular biology

Ines Martin-Martin,[1,6,8,*] Paola Carolina Valenzuela Leon,[1] Laura Amo,[2] Gaurav Shrivastava,[1] Eva Iniguez,[1] Azadeh Aryan,[3] Steven Brooks,[1] Bianca B. Kojin,[4] Adeline E. Williams,[1,5] Silvia Bolland,[3] Hans Ackerman,[1] Zach N. Adelman,[3,4] and Eric Calvo[1,7,9,*]

[1]Laboratory of Malaria and Vector Research, National Institute of Allergy and Infectious Diseases, National Institutes of Health, Rockville, MD 20852, USA
[2]Laboratory of Immunogenetics, National Institute of Allergy and Infectious Diseases, National Institutes of Health, Rockville, MD 20852, USA
[3]Department of Entomology and Fralin Life Science Institute, Virginia Polytechnic Institute and State University, Blacksburg, VA 24060, USA
[4]Department of Entomology, Texas A&M University, College Station, TX 77843, USA
[5]Department of Microbiology, Immunology, and Pathology, Colorado State University, Fort Collins 80523, CO, USA
[6]Present address: Laboratory of Medical Entomology, National Center for Microbiology, Instituto de Salud Carlos III, 28,220 Majadahonda, Madrid, Spain
[7]Twitter: @EricCalvoLab
[8]Twitter: @inemartinmartin
[9]Lead contact
*Correspondence: martinines@hotmail.com (I.M.-M.), ecalvo@niaid.nih.gov (E.C.)
https://doi.org/10.1016/j.celrep.2022.110648

SUMMARY

Saliva from mosquitoes contains vasodilators that antagonize vasoconstrictors produced at the bite site. Sialokinin is a vasodilator present in the saliva of *Aedes aegypti.* Here, we investigate its function and describe its mechanism of action during blood feeding. Sialokinin induces nitric oxide release similar to substance P. Sialokinin-KO mosquitoes produce lower blood perfusion than parental mosquitoes at the bite site during probing and have significantly longer probing times, which result in lower blood feeding success. In contrast, there is no difference in feeding between KO and parental mosquitoes when using artificial membrane feeders or mice that are treated with a substance P receptor antagonist, confirming that sialokinin interferes with host hemostasis via NK1R signaling. While sialokinin-KO saliva does not affect virus infection *in vitro*, it stimulates macrophages and inhibits leukocyte recruitment *in vivo*. This work highlights the biological functionality of salivary proteins in blood feeding.

INTRODUCTION

Aedes aegypti mosquitoes are the main vectors of yellow fever and dengue, Zika, and chikungunya viruses, which impose enormous burdens on human morbidity and mortality (Kauffman and Kramer, 2017; Souza-Neto et al., 2019). To ensure successful blood feeding, mosquito salivary contents counteract the three branches of host hemostasis: vasoconstriction, platelet aggregation, and coagulation. Mosquito saliva includes vasodilatory substances that antagonize vasoconstriction caused by the insertion of mouthparts during probing (Arca and Ribeiro, 2018; Ribeiro, 1987; Ribeiro and Arca, 2009). Vasodilators help hematophagy by increasing the amount of blood reaching the mouthparts and shortening the period of contact between the host and the arthropod (Andrade et al., 2005). A large diversity of vasodilators has been identified in the saliva of blood-feeding arthropods (Andrade et al., 2005). They include prostaglandins in ticks (Ribeiro et al., 1992), nitric oxide (NO) carried by nitrophorins in triatomines (Ribeiro et al., 1990), maxadilan in the sand fly *Lutzomyia longipalpis* (Lerner et al., 1991; Ribeiro et al., 1989), or adenosine and 5′-AMP in *Phlebotomus* sand flies (Ribeiro et al., 1999; Ribeiro and Modi, 2001). Anopheline mosquitoes do not produce vasodilatory substances, but rather secrete a catechol oxidase/peroxidase that destroys vasoactive amines and inactivates the physiologic vasoconstrictors of the host (Ribeiro and Nussenzveig, 1993). *Aedes aegypti* salivary glands contain sialokinins, vasodilatory peptides related to the tachykinin family, that stimulate endothelial cells to produce NO (Champagne and Ribeiro, 1994; Ribeiro, 1992) and are similar to the mammalian tachykinin substance P (Champagne and Ribeiro, 1994). Although the vasodilatory effect of sialokinins has been demonstrated *in vitro* (Champagne and Ribeiro, 1994; Ribeiro, 1992), no studies have unraveled its relevance *in vivo.* In this work, we demonstrated the vasodilator and immunomodulator effect of sialokinin by loss-of-function studies with two *Ae. aegypti* sialokinin knockout (KO) mosquito lines.

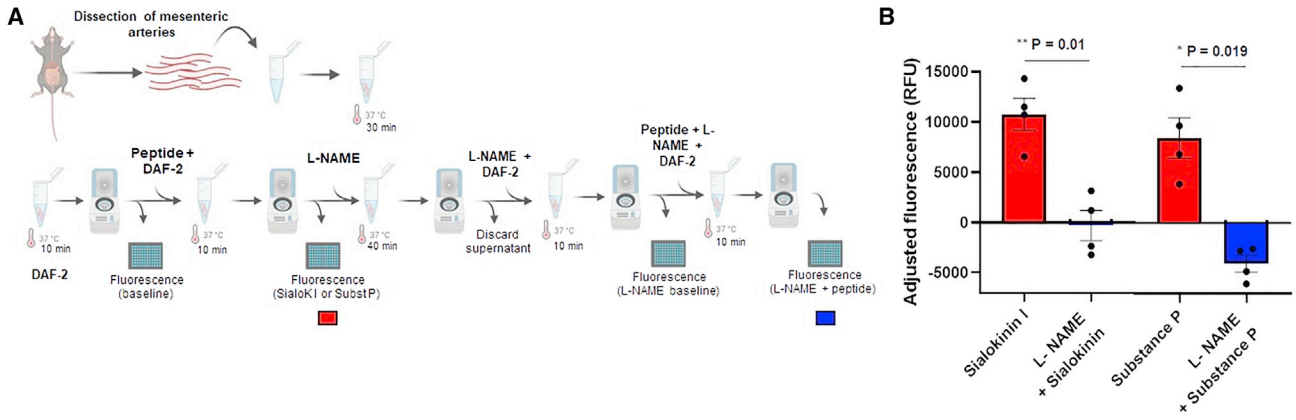

Figure 1. Determination of nitric oxide release by sialokinin I

(A) Diagram of the workflow used for the *ex vivo* detection of NO production by mouse mesenteric arteries.

(B) Graph shows the adjusted fluorescence as relative fluorescence units (RFUs) in the presence of sialokinin I or substance P with (blue) and without (red) L-NAME. The adjusted fluorescence was calculated as the fluorescence at wavelengths Ex_{485} and Em_{538} minus the correspondent baseline reading from each set of arteries. Baseline readings were assigned to the fluorescence readouts from arteries incubated with either DAF-2 in KH buffer or L-NAME, DAF-2 in KH buffer for each set of arteries. Each point represents the adjusted fluorescence from ~15 pooled arteries dissected from an individual mouse. Two independent experiments of 2 mice per peptide were included. Bars indicate SEMs. A paired t test was used to determine the statistical significance comparing treatments with or without L-NAME; *$p < 0.05$; **$p < 0.01$.

RESULTS

Sialokinin induces NO release by blood vessels

Due to the similarity of sialokinin to substance P, it was assumed, but never demonstrated, that sialokinin acts by stimulating endothelial cells to produce NO. We designed an *ex vivo* experiment to investigate whether blood vessels produced NO when treated with sialokinin or substance P (Figure 1A). Mouse mesenteric arteries take blood from the aorta and distribute it to the gastrointestinal tract. Mesenteric blood vessels incubated with sialokinin I peptide produced NO release in a manner similar to that of substance P, but the effect was abolished when arteries were treated with the antagonist of NO synthase (NOS) L-N^G-nitro arginine methyl ester (L-NAME) (Figure 1B). These results indicate that sialokinin I induces NO production through the activation of the NOS enzyme.

Generation of CRISPR-KO of *Ae. aegypti* sialokinin

To investigate the biological function of sialokinin, we generated sialokinin-KO mosquito lines. *Ae. aegypti* early-stage embryos were injected with Cas9 mRNA and a mixture of single-guide RNAs (sgRNAs; sgRNAs #1 and #2 or sgRNAs #3, #4, and #5; Figure S1A). Only samples derived from embryos injected with a combination of sgRNAs #1 and #2 showed a significant change in the fluorescence of the melting curve as compared with wild-type (WT) embryos, indicating the presence of mutations in injected embryos (Figure S1B).

To generate sialokinin-KO mosquito lines, 280 embryos were injected with Cas9 mRNA and a combination of sgRNAs #1 and #2. From these, 27 G_0 individuals survived to adult stages (9.64%; 10 females and 17 males). Two different mutations were identified in the exon 1 (Figure S1C). SialoK^{i5} corresponded to a 5-nucleotide insertion and sialoK$^{\Delta 8}$ corresponded to an 8-nucleotide deletion at the Cas9 cleavage point (Figure S1D). Both sialoK^{i5} and sialoK$^{\Delta 8}$ were expected to be loss-of-function mutant strains because the frameshift leads to the introduction of unrelated amino acids into the protein, followed by early stop codons (Figure S1E).

KO mosquitoes do not produce sialokinin

Peptides covering 93.55% of the sialokinin pro-protein were detected by mass spectrometry (MS) in the salivary glands of WT mosquitoes (Figure 2A), but peptides derived from sialokinin were absent in the salivary glands of sialoK^{i5} and sialoK$^{\Delta 8}$ mosquitoes (Figures 2A and 2B). Peptides detected in WT mosquitoes included part of the active decapeptide and one more amino acid in the N-terminal, indicating the presence of both pro-sialokinin I and the cleaved and active decapeptide in the salivary gland extracts (SGEs). The presence of pro-protein and the active decapeptide corresponding to sialokinin I was also confirmed in saliva collected from WT mosquitoes (Figure 2B). Only the decapeptide sialokinin I was identified (NTGDKFYGLM) in the salivary glands and saliva of WT mosquitoes. Sialokinin II, which only differs from sialokinin I in the first amino acid (DTGDKFYGLM), was not identified in our samples. Previously described allelic differences of the *sialokinin I* gene (Beerntsen et al., 1999) were located on nucleotides corresponding to the precursor protein sequence (pro-sialokinin), but not to the active decapeptide. These allelic variations were confirmed at the protein level because we detected all of the previously described variants in the SGE of WT mosquitoes by MS (Figure 2A). The genomic mutations of the *sialokinin I* gene caused by CRISPR-Cas9 did not significantly change the proteome of the salivary glands, as assessed by the diversity and abundance of salivary peptides detected in WT and mutant SGEs (R^2 = 0.9576) and saliva (R^2 = 0.9568) (Figures 2C and 2D). Whole proteomes from SGEs and saliva from either WT or sialokinin-KO mosquitoes are detailed in Tables S1 and S2, respectively.

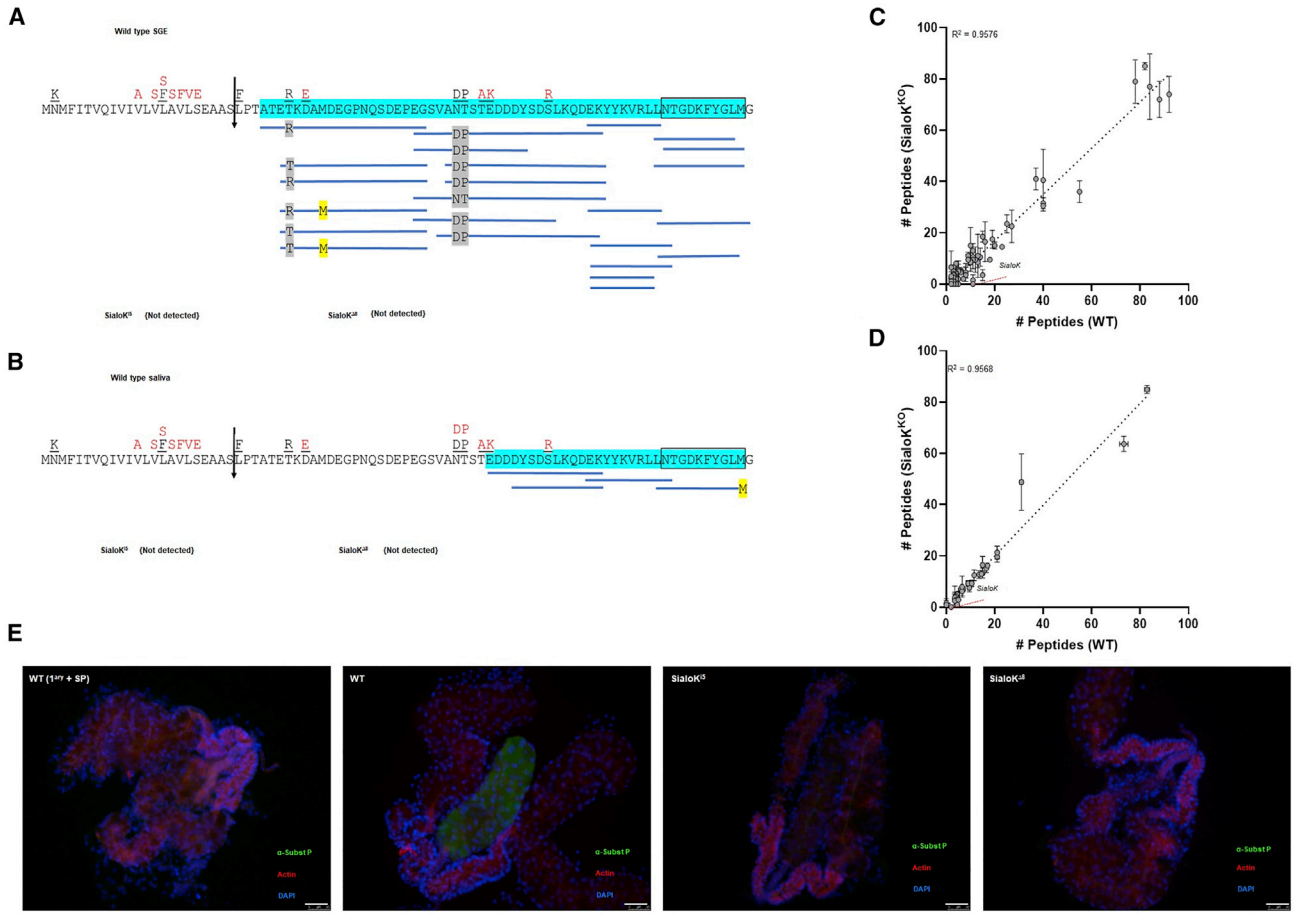

Figure 2. Mass spectrometry and immunofluorescence of salivary glands from KO mosquitoes

(A and B) Coverage map of sialokinin from (A) SGE obtained from 10 mosquitoes or (B) saliva from 50 mosquitoes by MS/MS. The vertical arrow denotes the predicted secretory cleavage site. Differences in the putative translation product between the cDNA sequence and the genomic sequence are located above the individual amino acids in black (Beerntsen et al., 1999) and red (Ribeiro et al., 2016). A total of 93.55% or 50% of the mature pro-sialokinin sequence was detected by MS/MS (highlighted in blue) in the SGE or saliva, respectively. The active sialokinin decapeptide is boxed. No peptides that matched sialokinin were detected in SGEs or saliva from either sialoK^{i5} or sialoK$^{\Delta 8}$ mosquitoes.

(C and D) Number of unique mapping peptides from SGE (n = 10) or (D) saliva samples from WT and KOs (2 sets of 50 salivating mosquitoes each). For differential expression analysis, the number of unique mapping peptides from sialoK^{i5} and sialoK$^{\Delta 8}$ was combined. Linear regression line and corresponding R^2 value are indicated. Bars indicate SDs.

(E) Immunolocalization of sialokinin in the salivary glands of female mosquitoes. A substance P-like protein was not detected in the salivary glands of sialoK^{i5} and sialoK$^{\Delta 8}$ KO mosquitoes. As a negative control (WT 1^{ary} + SP), salivary glands from WT mosquitoes were incubated with anti-substance P primary antibody pre-adsorbed with substance P. Merged fluorescence images are shown in green (anti-substance P; fluorescein isothiocyanate [FITC]), red (phalloidin Alexa Fluor 647), and blue (DAPI). Scale bars, 50 μm.

Immunofluorescence assays further supported the absence of sialokinin in the salivary glands of KO mosquitoes (Figure 2E). A substance P-related protein was localized in the medial lobe only in the salivary glands of WT mosquitoes. The positive signal was specific for a tachykinin-like recognition, since the signal was abrogated when the primary antibody was pre-incubated with excess substance P.

Sialokinin-KO mosquitoes show longer probing times on vertebrate hosts

Both sialokinin-KO mosquitoes (sialoK^{i5} and sialoK$^{\Delta 8}$) showed extended probing times when fed on mouse or chicken but not when fed using an artificial membrane feeder (Figures 3A–3D). However, when mice were pre-injected with the substance P receptor (NK1R) antagonist aprepitant, WT mosquitoes did not show an extended probing time, and the time was comparable to the probing time of KO mosquitoes ($p > 0.05$). KO mosquitoes that fed on chicken also showed prolonged probing times. However, when mosquitoes were blood fed using an artificial membrane system with bovine blood, no significant differences in probing time were found among mosquito groups (Figures 3C–3E). These results suggest that sialokinin contributes to shorten probing times in vertebrates, possibly through neurokinin-1 receptor (NK1R) signaling. However, more research is needed to understand the mechanism of sialokinin in NO release.

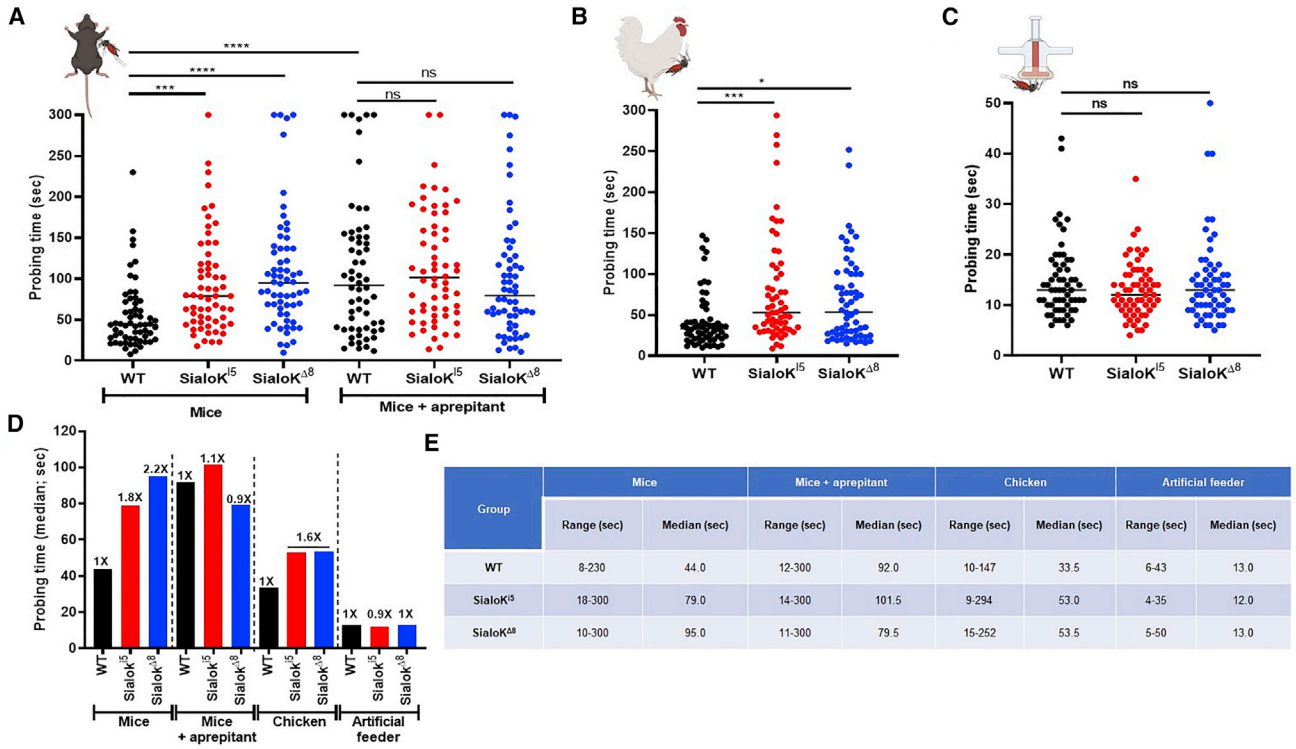

Group	Mice		Mice + aprepitant		Chicken		Artificial feeder	
	Range (sec)	Median (sec)	Range (sec)	Median (sec)	Range (sec)	Median (sec)	Range (sec)	Median (sec)
WT	8-230	44.0	12-300	92.0	10-147	33.5	6-43	13.0
SialoK^{I5}	18-300	79.0	14-300	101.5	9-294	53.0	4-35	12.0
SialoK$^{\Delta 8}$	10-300	95.0	11-300	79.5	15-252	53.5	5-50	13.0

Figure 3. Probing time analysis in sialokinin-KO *Aedes aegypti*

(A–C) Individual mosquitoes were monitored for probing time experiments in mice without or with intraperitoneal (i.p.) injections of the substance P receptor antagonist aprepitant (A), chicken (B), and artificial membrane feeders (C). For each plot, samples were compared using either a 1-way ANOVA for normal distributed samples or a non-parametric test Kruskal-Wallis test for non-normal distributed samples. For multiple comparisons, WT was used as the control group. The p value indicates the result of the ANOVA test: ns: $p > 0.05$; *$p < 0.05$; **$p < 0.01$; ***$p < 0.001$; ****$p < 0.0001$.

(D) Data from (A)–(C) expressed as fold change compared to WT mosquitoes.

(E) Probing time parameters for sialokinin-KO mosquitoes on mice, chickens, and artificial membrane feeder. Two independent experiments with a total of at least 60 mosquitoes were assayed per group.

Sialokinin-KO mosquitoes have reduced blood-feeding success but no alteration of fecundity and fertility

Since sialokinin-KO mosquitoes presented longer probing times, we also investigated blood-feeding success, determined as the percentage of engorged mosquitoes after 90 or 120 s. Using mice as a host, we found a significant decrease in the percentage of blood-fed mosquitoes in the sialokinin-KO groups compared to WT, both after 90 and 120 s of blood feeding (Figures 4A and 4E). However, no significant difference was observed between groups when aprepitant pre-treated mice were used (Figures 4B and 4F). These results indicate that sialokinin contributes to blood-feeding success through the NK1 receptor. In chickens, both sialoK^{i5} and sialoK$^{\Delta 8}$ mosquitoes showed lower blood feeding rates compared to WT mosquitoes, with sialoK$^{\Delta 8}$ mosquitoes showing the lowest blood-feeding success (Figures 4C and 4G). No differences in blood-feeding success rates were found when mosquito groups were fed using an artificial membrane system with bovine blood (Figures 4D and 4H). When experiments were carried out on mice at longer times (4 min), no differences in feeding rates were observed across groups (Figure S2).

No significant difference in blood meal size was observed across mosquito groups in experiments performed on mice or chickens (Figures S3A–S3D), indicating that sialokinin exclusively influences probing without affecting blood ingestion. From the feeding success experiments (Figure 4), sets of blood-fed mosquitoes on mice and chickens were used to determine fecundity (number of eggs laid) and fertility (number of eggs hatched) parameters. No differences in the number of eggs laid per mosquito or the number of eggs hatched were found across mosquito groups (Figures S3E–S3L). Overall, these results show that mosquitoes that imbibe comparable amounts of blood have similar fecundity and fertility parameters independent of the presence of sialokinin.

The saliva of sialokinin-KO mosquitoes is not able to induce vasodilation *in vivo*

We determined the effect of sialokinin on host vasculature during a mosquito bite using laser speckle contrast imaging to analyze blood flow at the bite site (Figure 5A). We observed an increase in blood perfusion at the bite site during probing, feeding, and 2 min post-feeding of WT mosquitoes (Figures 5B and 5C), which was visualized in our experiments as an accumulation of red signal. The bite of sialokinin-KO mosquitoes produced lower blood perfusion during probing and feeding (Figure 5C).

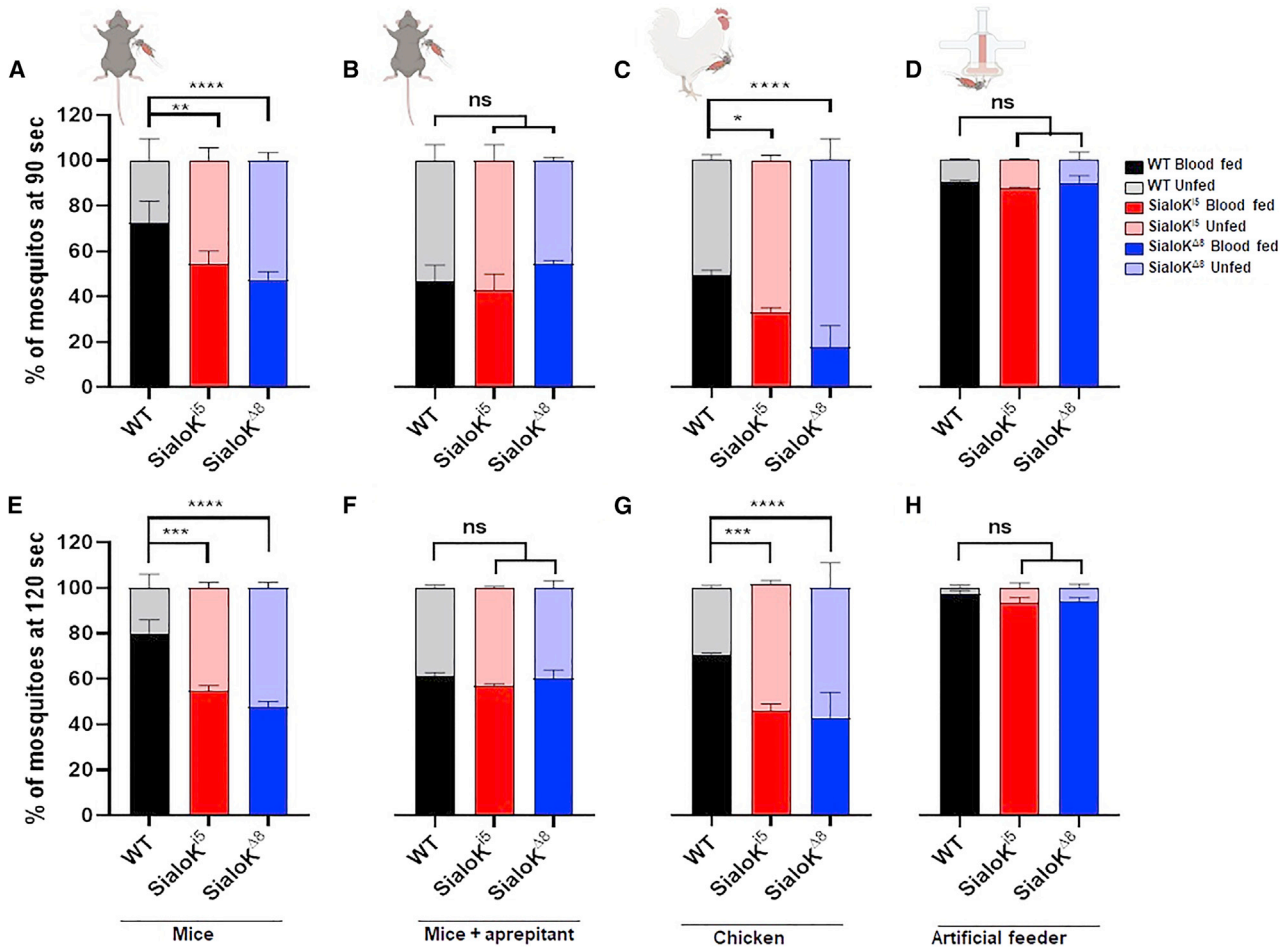

Figure 4. Feeding success analysis in sialokinin-KO *Ae. aegypti*

Blood-feeding success rate: percentage of blood-fed females after 90 (A–C) or 120 s (D–F) in WT (black) and KO mosquitoes (sialoK^{i5}, red, and sialoK$^{\Delta 8}$, blue). Feeding success rates were determined in mice without (A and E) or with injections of aprepitant (B and F), chicken (C and G), and artificial membrane feeders (D and H). Feeding status data are presented as mean values of 2 independent experiments carried out by different operators. Each independent experiment consisted of 2 biological replicates of 100 mosquitoes each. Bars indicate SEMs. Contingency analyses were performed by chi-square and Fisher tests. For multiple comparisons, WT was selected as the control group. The p value indicates the result of the chi-square test: ns: $p > 0.05$; *$p < 0.05$; **$p < 0.01$; ***$p < 0.001$; ****$p < 0.0001$.

See also Figure S3.

We performed similar analyses by the intradermal inoculation of SGEs collected from sialokinin-KO *Ae. aegypti.* Our results showed that SGEs from WT mosquitoes induced greater vasodilation 1 and 2 min post-injection than SGEs from both sialokinin-KO mosquitoes (Figures 5D–5F). These results demonstrate that sialokinin is the main salivary vasodilator in *Ae. aegypti*.

The saliva of sialokinin-KO mosquitoes inhibits leukocyte recruitment to the bite site and modulates macrophage response without affecting Zika virus infection

Numerous studies reported a positive effect of *Ae. aegypti* saliva on virus infection (Hastings et al., 2019; Schmid et al., 2016; Sun et al., 2020). Salivary components can elicit immune responses both at the bite site (Guerrero et al., 2020; Henrique et al., 2019) and systemically (Assis et al., 2021; Vogt et al., 2018; Zeidner et al., 1999). Sialokinin has a profound effect on interferon-γ (IFN-γ) and interleukin-2 (IL-2) production by cultured splenocytes (Zeidner et al., 1999) and enhances Semliki Forest virus (SFV) infection in mice (Lefteri et al., 2021). However, little is known about the exact role of sialokinin on the host immune response during mosquito blood feeding. Other members of the tachykinin family proteins, such as substance P or hemokinins, induce angiogenesis and enhance cellular immunity responses through NK1R signaling (expressed in immune cells) (Song et al., 2012). In fact, substance P acts as a mediator of cross-talk between the nervous and immune systems in mammals and promotes the migration and extravasation of several immune cells (Choi and Di Nardo, 2018; Hodo et al., 2020; Suvas, 2017). Therefore, we further investigated the role of sialokinin on host immunology and Zika virus (ZIKV) infection by comparing the effect of the SGEs from KO and WT mosquitoes.

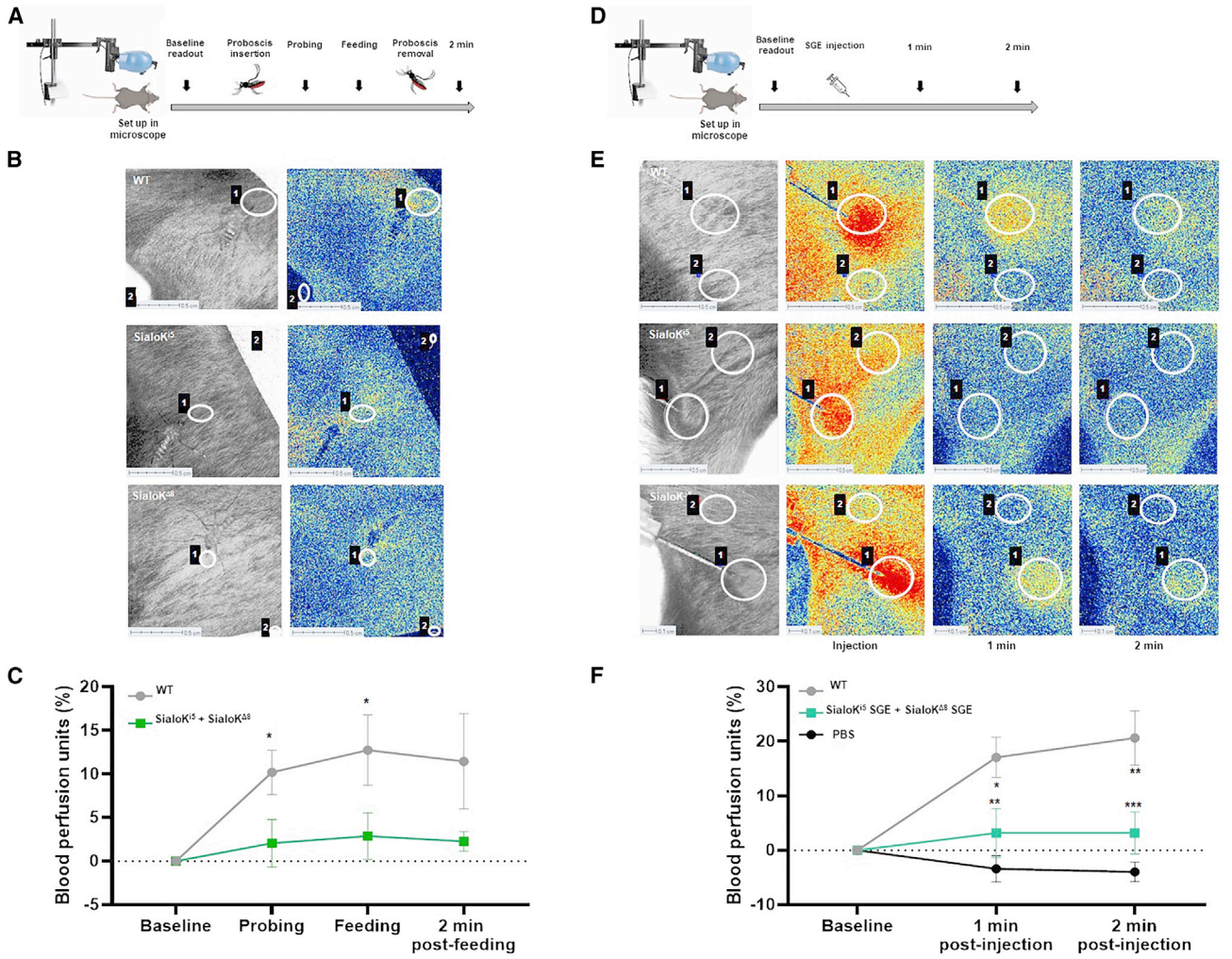

Figure 5. Analysis of skin perfused blood during a mosquito bite or SGE inoculation from sialokinin-gene edited *Ae. aegypti*

(A) Diagram of workflow of laser speckle experiments during a mosquito bite.

(B) Speckle tissue perfusion images of mouse lower back during WT or KO mosquito bites (sialoK^{i5} and sialoK$^{\Delta 8}$).

(C) Graphs showing the blood perfusion units in each group during probing, feeding, and 2 min post-feeding. High blood perfusion is visualized in red and low blood perfusion is in blue. The results were normalized to the blood perfusion units at the bite site before probing and are shown as the mean of measurements of 10 mosquitoes per group (WT, sialoK^{i5}, and sialoK$^{\Delta 8}$) ± SEMs. The results from sialoK^{i5} and sialoK$^{\Delta 8}$ were combined for representation and analysis.

(D) Diagram of workflow of laser speckle experiments during injection of SGE.

(E) Speckle tissue perfusion images of mouse lower back during injection of SGE from WT or KO mosquitoes.

(F) Graphs showing the blood perfusion units in each group before and 1 min and 2 min after SGE injection. The results were normalized to the blood perfusion units at the inoculation site before SGE injection. The results are shown as the mean of 6 injections per group ±SEMs. The results from sialoK^{i5} and sialoK$^{\Delta 8}$ were combined for representation and analysis. Two regions of interest were selected: the mosquito biting or injection area (1) and a control area separated from the bite or injection (2). Each mosquito bite or injection corresponded to 1 biological replicate. Regions of interest selected as controls always remained lower than 2 blood perfusion units. Scale bar, 0.5 cm. A 2-way ANOVA test was used to determine the statistical significance. Multiple comparisons were made among treatments for each time point; ns: $p > 0.05$; *$p < 0.05$; **$p < 0.01$; ***$p < 0.001$; ****$p < 0.0001$.

To study the effect of sialokinin on leukocyte recruitment, we injected PBS or SGE from WT or sialokinin-KO mosquitoes in C57BL/6 mice footpads and quantified the number of leukocytes recruited to the footpad area. Using flow cytometry, we measured tissue-recruited leukocytes (CD45$^+$ cells), which doubled in number the PBS-injected group 24 h after WT SGE injection (Figure 6A). In contrast, footpads from mice injected with sialokinin-KO SGEs had significantly reduced numbers of recruited leukocytes (Figure 6A) compared to footpads injected with WT SGE. Myeloid cells (CD45$^+$CD11b$^+$) and T cells (CD45$^+$CD3$^+$) were significantly reduced in sialokinin-KO SGE-injected footpads compared to WT SGE injections, while B cells (CD45$^+$CD19$^+$) and mast cells (CD45$^+$cKit$^+$FceR1a$^+$) remained similar. Further analysis of myeloid and T cells revealed that the neutrophils (Ly6C^{dim}Ly6G$^+$) and CD8$^+$ T cells were the main populations that were significantly reduced after

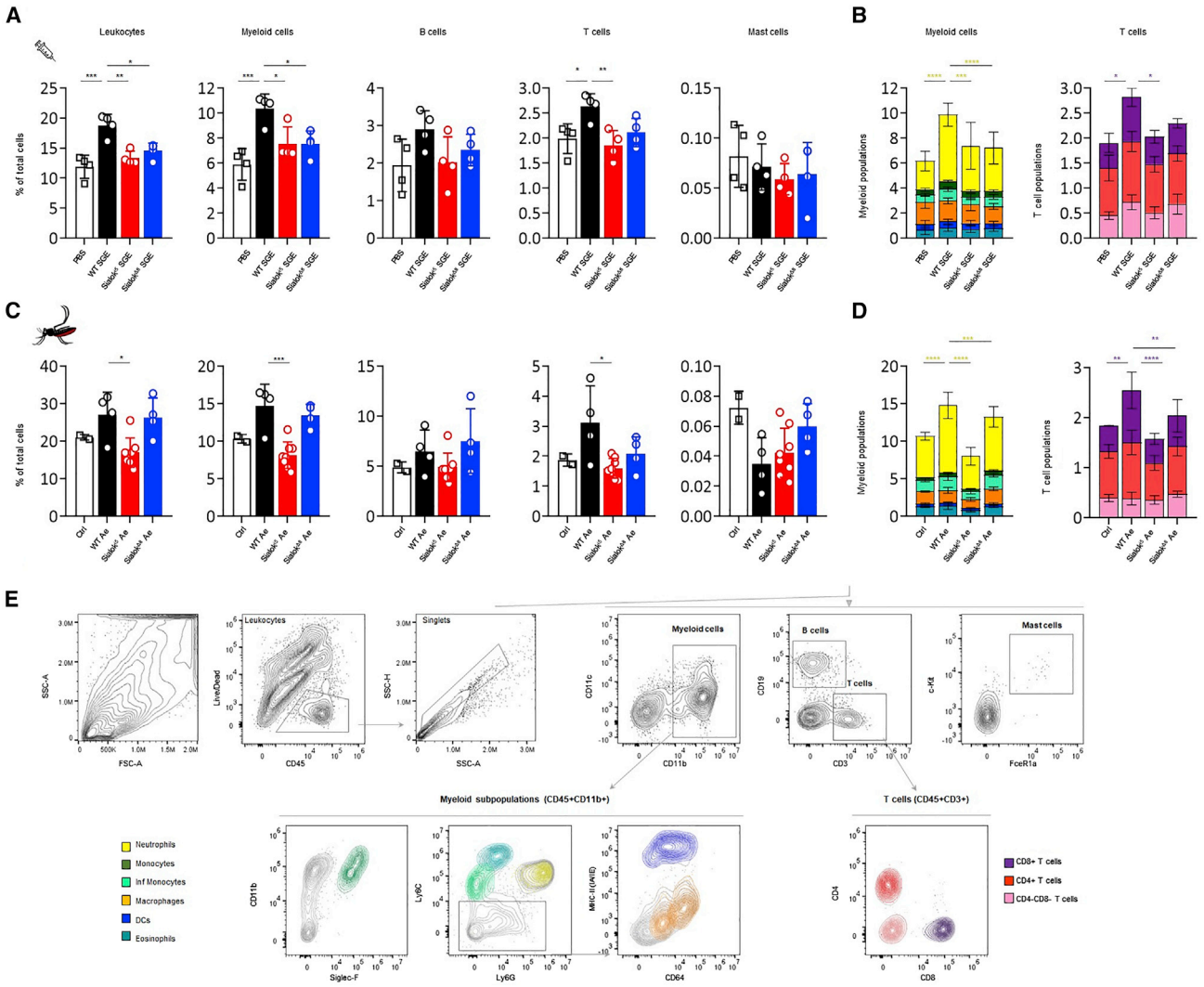

Figure 6. Host leukocyte recruitment to the SGE injection site or mosquito bite site using sialokinin-KO *Ae. aegypti*

Flow cytometry analysis of leukocytes present in the footpad of mice 24 h after SGE injection (A and B) or mosquito bites (C and D).

(A) Graphs showing the percentage of leukocyte populations per mouse footpad 24 h after the injection of 6 μg SGE from WT or sialokinin-KO mosquitoes (same volume of PBS was injected in control animals: 40 μL) or (C) mosquito bites. Non-bitten footpads were used as controls.

(B and D) Combined graphs showing the distribution of myeloid or T cell subpopulations as a percentage of cells per footpad. Four mice per group were used.

(E) Flow cytometry gating strategy and color coding. Subpopulations were selected from leukocyte ($CD45^+Live/Dead^-$) singlets as follows: myeloid cells ($CD11b^+$); eosinophils ($CD11b^+SiglecF^+$, blue-green); monocytes ($CD11b^+Ly6C^+$, light green); inflammatory monocytes ($CD11b^+Ly6C^{hi}$, dark green); neutrophils ($CD11b^+Ly6G^+$, yellow); macrophages ($CD11b^+Ly6C/G^-CD64^+$, orange); dendritic cells (DCs, $CD11b^+Ly6C/G^-MHC\text{-}II^{hi}$ $CD11c^+$, dark blue); B cells ($CD19^+$); mast cells ($CD45^+CD11b^-CD3^-CD19^-cKit^+FceR1a^+$); and $CD4^+$ (dark red), $CD8^+$ (purple), or $CD4^-CD8^-$ (pink) T cells ($CD3^+$). Four to eight samples were included in each experimental group. Each sample corresponds to 1 footpad. The results are indicated as the means ± SDs. One- (A and C) and 2-way (B and D) ANOVA tests were used to determine statistical significance. For multiple comparisons, the injection of WT SGE or bites of WT mosquitoes (WT Ae) were used as control groups. p values are indicated: ns: $p > 0.05$; *$p < 0.05$; **$p < 0.01$; ***$p < 0.001$; ****$p < 0.0001$.

See also Figure S4.

sialokinin-KO SGE injection compared to sialokinin WT SGEs (Figure 6B).

To determine whether this effect occurs during blood feeding, we performed similar analyses after exposing mice footpads to *Ae. aegypti* bites for 15 min (Figure 6C). We confirmed the results obtained with SGE inoculations, with a significant reduction of neutrophils and $CD8^+$ T cells 24 h after exposure to sialokinin-KO mosquitoes. We did not observe a significant reduction in B cells or mast cells at the bite site (Figure 6D). These results suggest that sialokinin contributes to the leukocyte recruitment observed in the WT group, specifically to the recruitment of neutrophils and $CD8^+$ T cells.

The immunomodulatory function of substance P was also described *in vivo* and *in vitro* by its proinflammatory effect on

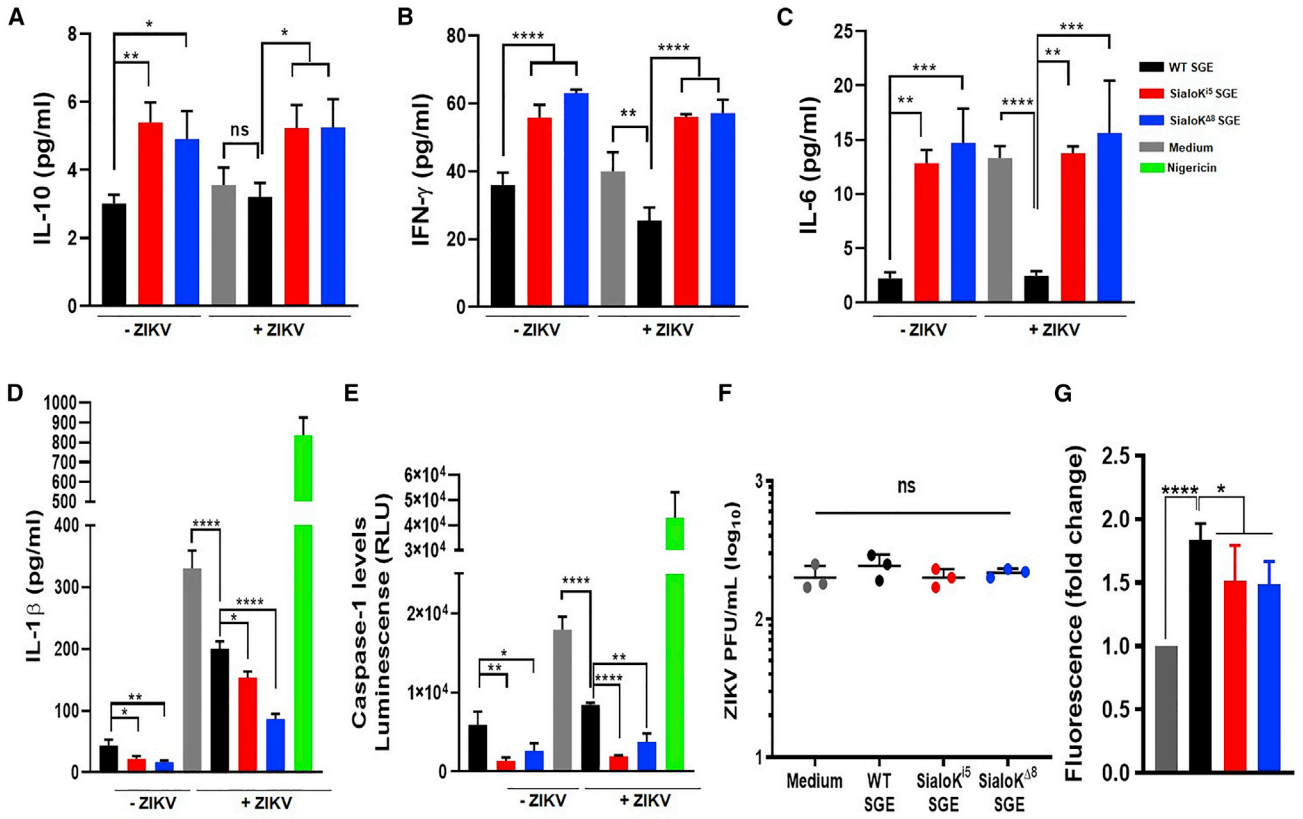

Figure 7. Effect of sialokinin-KO SGE in macrophages during ZIKV infection

(A–E) Macrophages were treated with SGE from WT, sialoK^{i5}, and sialoK$^{\Delta 8}$ mosquitoes in the absence or presence of ZIKV. As positive controls, cells were treated with nigericin. The levels of IL-10 (A), IFN-γ (B), IL-6 (C), IL-1β (D), and caspase (E) presented as the means ± SDs of a triplicate from a representative of 3 independent experiments (n = 3).

(F) Virus titers of supernatants from macrophages infected with ZIKV in the presence of SGE from WT, sialoK^{i5}, or sialoK$^{\Delta 8}$ mosquitoes ±SDs. Biological triplicates are shown. PFU, plaque-forming unit.

(G) Effect of SGE from sialokinin-KO mosquitoes on endothelial permeability. FITC-dextran permeability is expressed as a fold increase over the control (only medium) ± SDs. The data from 2 independent experiments performed in duplicate are shown. One-way ANOVA tests was used to determine statistical significance. For multiple comparisons, WT SGE was selected as the control group. ns: $p > 0.05$; *$p < 0.05$; **$p < 0.01$; ***$p < 0.001$; ****$p < 0.0001$.

leukocytes such as macrophages (Hodo et al., 2020). This effect can have an impact in the infective process of viruses transmitted by *Ae. aegypti* such as ZIKV. We observed an increase in IL-10, IFN-γ, and IL-6 levels and a reduction in IL-1β in macrophages treated with sialokinin-KO SGE compared to cells treated with SGE from WT mosquitoes (Figures 7A–7D). Like IL-1β, caspase-1 levels were reduced in macrophages treated with sialokinin-KO SGE (Figure 7E). These effects were more evident when cells were infected with ZIKV (Figures 7D and 7E). However, in our *in vitro* system, SGE from WT or sialokinin-KO did not have an effect on the ZIKV infection of macrophages because viral titers were similar across groups (Figure 7F).

The saliva of sialokinin-KO mosquitoes shows lower endothelial permeability enhancement

Mosquito salivary components contribute to skin endothelial permeability during blood feeding (Schmid et al., 2016). Host endothelial permeability consists of increased edema and attraction of immune cells at the bite site; in this environment, red blood cell density is reduced, leading to a less nutritious blood meal for the mosquito. Sialokinin enhanced arboviral infection in mice, which was attributed to the disruption of the endothelial barrier (Lefteri et al., 2021). Our results showed that SGEs from WT mosquitoes significantly increased endothelial permeability at 30 min (Figure 7G). However, SGEs from sialokinin-KO mosquitoes showed a reduced cell permeability. These results confirm the contribution of sialokinin in the endothelial permeability enhancement observed in the WT SGE group.

DISCUSSION

The vasodilator present in *Ae. aegypti* salivary glands, sialokinin, was discovered in the early 1990s through a combination of saliva fractionation and functional vasodilation assays (Ribeiro, 1992). It is a peptide related to the mammalian tachykinin substance P that acts either as a neurotransmitter released from the nerve ending after a calcium-dependent mechanism or as

autocrine, paracrine, or endocrine regulators released by non-neuronal cells (Severini et al., 2002). Substance P elicits a spectrum of biological activities depending on the location of its receptor. The activation of tachykinin receptors on blood vessels leads to the release of vasodilator agents from the endothelium, causing vasodilation, a function shared with the mosquito sialokinin. The immunomodulatory effects of substance P have been described *in vivo* and *in vitro* (Hodo et al., 2020).

In this work, we successfully generated two homozygous KO lines (sialoK^{i5} and sialoK$^{\Delta 8}$) in which sialokinin protein expression was abolished, as confirmed by immunofluorescence and MS in both SGE and saliva collected from KO mosquitoes. Based on tandem MS (MS/MS) results, overall peptide diversity and abundance in SGEs and saliva from sialokinin-KO lines were similar to those of WT mosquitoes, with no evidence of compensatory factors up- or dow-regulated in response to the loss of sialokinin.

Like mammalian tachykinins (Severini et al., 2002), sialokinin I is expressed as a precursor (prepro-sialokinin) and post-translationally processed (Beerntsen et al., 1999). Previous work identified two sialokinin peptides in the salivary glands of *Ae. aegypti*, differing only in the amino acid present at the N terminus: asparagine in sialokinin I and aspartic acid in sialokinin II (Champagne and Ribeiro, 1994). It was suggested that both peptides originated from allelic variations of the same gene. However, after extensive sequencing attempts with cDNA clones, Beerntsen et al. (1999) could not prove that polymorphisms of the *sialokinin I* gene accounted for the presence of sialokinin II. Using RNA sequencing (RNA-seq) analyses of a salivary gland transcriptome, no gene that codified sialokinin II was found (Ribeiro et al., 2016). So far, only the *sialokinin I* gene (GenBank: AF108099; VectorBase: AAEL000229), which was present on chromosome I of the mosquito as a single-copy gene, has been identified (Beerntsen et al., 1999; Giraldo-Calderon et al., 2015). Previous studies postulated that sialokinin II may be a degradation product of sialokinin I that occurs either naturally or as a result of the isolation procedure (Beerntsen et al., 1999). However, we only identified sialokinin I in SGEs and secreted saliva, supporting the hypothesis of the natural presence of only sialokinin I.

At present, the processing from prepro-sialokinin to the active decapeptide is not fully understood. Signal peptidases likely cleave the signal peptide and direct the pro-sialokinin to the secretory pathway. The typical cleavage site points are Lys-Arg, Arg-Arg, and Arg-Lys doublets (Steiner et al., 1992). However, endopeptidases have not been well described in insects, and cleavage of sialokinin I is predicted to occur after a Leu-Leu doublet. In our MS/MS studies, we identified peptides covering the mature decapeptide and the pro-sialokinin in both SGEs and saliva. The third step of processing requires the removal of the terminal Gly that would likely occur by a peptidyglycine α-amidating mono-oxygenase (Kolhekar et al., 1997), even though the presence of these enzymes has not been demonstrated in mosquitoes. This terminal Gly is not present in sialokinin detected from SGE or saliva.

Tachykinin-like vasodilator activity was seen in the salivary glands of *Ae. triseriatus* (Ribeiro et al., 1994). It is not clear how *Ae. aegypti* and *Ae. triseriatus* may have acquired a vasodilator peptide similar to a vertebrate neuropeptide. Horizontal gene transfer has provided new tools for blood-feeding arthropods. The cysteine and tryptophan-rich protein family found in *Culex* (Kern et al., 2021; Ribeiro et al., 2004), *Psorophora* (Chagas et al., 2013), and *Corethrella* genuses (Ribeiro et al., 2014), and the vasodilator hormone vasopresin found in *Ornithodoros* ticks, have been acquired through horizontal gene transfer from prokaryotes (Kern et al., 2021; Ribeiro et al., 2004) and from the vertebrate host, respectively (Iwanaga et al., 2014). The *Ae. aegypti* sialokinin sequence is similar to the vertebrate tachykinins, especially at the C-terminal region that specifically interacts with the receptor. However, analysis of the *sialokinin I* gene reveals that this peptide is not homologous, but rather analogous, to vertebrate tachykinins, and it may have arisen through convergent evolution to resemble a peptide with vasodilator properties (Champagne and Ribeiro, 1994).

Our experiments showed that sialokinin is a relevant peptide that facilitates vertebrate blood feeding because probing time and feeding success were altered in the absence of sialokinin. In contrast, sialokinin-KO mosquitoes could feed normally on anticoagulated bovine blood through artificial membrane feeders, demonstrating that sialokinin functions specifically to prevent host hemostasis. Blood-feeding arthropods must keep probing time short to minimize host immune responses that trigger host awareness to the mosquito. While we observed that sialokinin-KO mosquitoes were eventually able to obtain a full blood meal given sufficient time, all of the feeding experiments were done on anesthetized and immobilized animals, in which consequences to host alertness to mosquito presence have been eliminated. An experiment in which mosquitoes attempt to blood feed on animals that are fully awake would provide a better scenario of what would happen in nature, particularly with human hosts who defend themselves from mosquitoes once alerted. Feeding success experiments with the KO mosquitoes followed a similar trend.

From the blood feeding on mice and chickens, we did not observe any difference in hemoglobin content between the WT and sialokinin-KO mosquitoes, indicating that in the absence of sialokinin, mosquitoes take longer to locate the blood vessels; however, once they find a blood vessel and start feeding from it, they are able to ingest similar amounts of blood as WT. Blood-fed mosquitoes from WT and sialokinin-KO groups ingesting a similar volume of blood showed comparable fertility and fecundity parameters, supporting the lack of off-target effects derived from gene manipulation.

Laser speckle contrast imaging is a technique based on the dynamic change in the backscattered light resulting from the illumination of red blood cells by a laser light. It can be used to visualize blood perfusion in various tissues (Heeman et al., 2019; Seryogina et al., 2019). This is the first time this technique has been used to assess the microvascular blood flow during active mosquito feeding on a vertebrate host. Our laser speckle experiments confirmed that there is vasodilation in the skin microvasculature during a mosquito bite, and that it is fairly maintained after the bite. Sialokinin-KO mosquitoes failed to induce vasodilation at the bite site, especially during probing, when the sialokinin action is most important. Individual mosquito

feeding behavior led to increased experimental variability. Injection of SGE from the different mosquitoes showed a clearer and more robust effect on vasodilation between WT and sialokinin-KO. These data suggest that sialokinin is the main vasodilator in *Ae. aegypti* saliva. However, the inhibition of vasoconstriction at the bite site may be accomplished by other secreted salivary proteins such as D7-long proteins. Both AeD7L1 and AeD7L2 bind and scavenge host hemostatic agonists such as biolipids and norepinephrine and have been shown to inhibit the vasoconstriction that these agonists cause in mouse arteries (Martin-Martin et al., 2020).

Sialokinin was characterized as a tachykinin because of its sequence similarity to the mammalian tachykinins and its ability to dilate the rabbit aortic ring and contract the guinea pig ileum. The vasodilatory activity in the saliva of *Ae. aegypti* was shown to be endothelium dependent, heat stable, and sensitive to both trypsin and chymotrypsin treatments (Ribeiro, 1992). To investigate the actual mechanism of action of sialokinin, we studied the effect of blocking the neurokinin-1 receptor with the antagonist aprepitant (Mannangatti et al., 2017). Substance P is an endogenous NK1R agonist (Page, 2013), and we evaluated the effect on NK1R located in the blood vessel endothelium. Our experiments confirmed that the increased probing time and impaired blood feeding success observed for sialokinin-KO mosquitoes were a result of the sialokinin effect on the vertebrate tachykinin receptor. In addition, mouse mesenteric arteries produced NO upon incubation with either sialokinin or substance P, and its release was diminished when the antagonist of NOS L-NAME was added. A biological phenomenon is taken to be NOS dependent and NO mediated if it is reduced or eliminated by the addition of a NOS inhibitor (Griffith and Kilbourn, 1996). L-NAME is an L-arginine analog widely used as a NOS inhibitor (Griffith and Kilbourn, 1996). NOS catalyzes the conversion of L-arginine to NO (Moncada and Higgs, 1993), and both type II (cytokine inducible: iNOS) and type III (endothelial constitutive: eNOS) have been found in endothelial cells (Galley and Webster, 2004; Laurindo et al., 2018). Constitutive production of NO by eNOS controls the vasculature tone and regulates blood pressure and organ perfusion. We confirmed the sialokinin mechanism of action through our *in vivo* and *ex vivo* experiments. Sialokinin functions as an agonist of the NK1R located in the vasculature endothelial cells, which triggers the activation of eNOS, releasing NO that causes dilation of the blood vessel smooth muscle.

A role for sialokinin in host immunity was first observed by Zeidner et al. (1999), who showed that splenocytes from sialokinin-injected mice skewed their immune responses toward a Th2 phenotype similar to the whole SGE. During the preparation of this manuscript, an extensive preprint on host immunology against sialokinin was deposited in the BioRxiv repository. The authors showed that sialokinin enhanced virus infection *in vivo* by impairing endothelial barrier integrity (Lefteri et al., 2021). In our experiments, SGE altered endothelial permeability at 30 min. These results match the observations of Lefteri et al., which found that *Ae. aegypti* saliva disrupted barrier function within 1 h (Lefteri et al., 2021). Together with the effect on vascular permeability, we found that sialokinin induces vasodilation at the bite site and contributes to NO release. These mechanisms may positively influence leukocyte recruitment to the bite site. Similar functions were described for substance P in vascular permeability (Nguyen et al., 1995), as well as in corneal epithelial cell tight junctions or the nervous system (Araki-Sasaki et al., 2000; Ko et al., 2009a, 2009b; Suvas, 2017; Yang et al., 2016). As a part of the tachykinin family, and specifically due to similarities between sialokinin and substance P, it is possible that sialokinin has an immunomodulatory role similar to that of substance P. The effect of substance P in local and systemic inflammation has been described in several studies (Suvas, 2017). Substance P not only facilitates leukocyte extravasation and migration, but it can act directly to modulate inflammatory responses in specific cells such as monocytes and macrophages (Suvas, 2017). A recent study revealed that substance P injection increased neutrophil and monocyte recruitment to the injection site in mice at 24 h (Green et al., 2019). Our leukocyte recruitment experiments after SGE inoculation or through bite of the KO mosquitoes suggest that sialokinin contributes to the recruitment of neutrophils, $CD8^+$ T cells, and $CD4^+$ T cells. It is well known that neutrophils are the first cells to arrive to the bite site, becoming the first line of defense against skin pathogens (Pingen et al., 2016). They can eliminate pathogens by direct mechanisms (phagocytosis, release of cytotoxic molecules, and formation of neutrophil extracellular traps) or indirectly by attracting other leukocytes such as monocytes and lymphocytes. Among these, $CD8^+$ T cells also respond to intracellular pathogens through direct cytotoxicity against infected cells. However, leukocyte recruitment can result in an increased number of permissive cells to the virus, enhancing viral load locally, which agrees with other studies (Hastings et al., 2019; Lefteri et al., 2021).

Our experiments with macrophages allowed us to assess the direct immunomodulatory effect of sialokinin during ZIKV infection. Sialokinin inhibits the production of inflammatory cytokines and activates two important components of the inflammasome pathway: IL-1β and caspase-1. Similar macrophage modulation was found in substance P *in vitro* and *in vivo* in spinal cord injury (Jiang et al., 2012; Lim et al., 2017; Montana and Lampiasi, 2016). Although the specific mechanism is not yet elucidated and varies depending on the type of study, substance P induces the expression of inflammatory cytokines in macrophages and contributes to macrophage activation. We did not observe any difference in ZIKV infection in macrophages in the presence or absence of SGEs from either WT or sialokinin-KO mosquitoes. These results agree with Lefteri et al. (2021), who showed that mosquito saliva had no effect on SFV infection of fibroblasts and macrophages in primary cultures. However, they did show that sialokinin enhanced virus infection *in vivo* by impairing the endothelial barrier integrity. Therefore, sialokinin is capable of directly modulating macrophage response, but it does not increase ZIKV infection *in vitro*. As Lefteri et al. (2021) suggested, sialokinin would contribute to ZIKV infection by altering endothelial permeability, which in turn would facilitate cell recruitment to the bite site. Increasing the number of cells susceptible to infection, together with a proinflammatory environment, favors viral replication at the bite site. Our results support the hypothesis that vasculature alteration induced by sialokinin contributes to

leukocyte recruitment and can have important consequences on viral replication.

In conclusion, we showed that the sialokinin mechanism of action induces vasodilation through the activation of NOS via NK1R signaling and disrupts the vasculature via enhanced endothelial permeability, similar to substance P. We demonstrated the relevance of sialokinin in blood feeding and host immunology through the generation of KO mosquitoes. In the absence of sialokinin, mosquito bites fail to produce substantial vasodilation; this is associated with longer probing times and lower feeding success. In addition, mosquitoes that lack sialokinin have a reduced ability to recruit leukocytes and activate macrophages, which has potential consequences on pathogen transmission.

Limitations of the study

We note several technical caveats when working with mosquito salivary proteins. First, the biological effect of a salivary protein should be studied using saliva rather than SGEs, which may contain proteins not secreted in mosquito saliva. However, saliva collection is a highly skilled and tedious process that involves the manipulation of individual mosquitoes. The use of SGEs, obtained after the homogenization of whole salivary glands following the separation of the gland walls by centrifugation, is generally accepted to study the effect of saliva; however, all of the researchers working in this field should bear in mind this potential limitation. Second, we would have preferred to show blood vessel NO release, not only with the sialokinin peptide but also with saliva or SGEs from WT and KO mosquitoes. However, we would need large amounts of SGE or saliva to be able to see an effect in this experimental setting. We detected an effect in our experiments when using peptide concentrations of 100 μM. This dose is too high when compared to what would be secreted by an individual mosquito. However, the bite size would be significantly smaller than the minimum volume of our assay, and the effect would be inscrutable because it would be below the limit of detection. Our goal was not to mimic the doses of sialokinin in nature but to demonstrate the function of sialokinin through an experiment that let us measure the NO release using whole arteries. To our knowledge, this is the best approach to investigate the NO release in an *ex vivo* experiment. Another caveat of studies that mimic mosquito blood feeding is the difficulty of standardizing the experimental setup-like variation in blood meal size, the number of mosquitoes that feed, or the membrane/animal feeding system. This is particularly important for the laser speckle and probing/feeding success experiments. We tried to reduce individual blood-feeding variation by starving female mosquitoes for 2 days so that they are eager to initiate feeding.

STAR★METHODS

Detailed methods are provided in the online version of this paper and include the following:

SUPPLEMENTAL INFORMATION

Supplemental information can be found online at https://doi.org/10.1016/j.celrep.2022.110648.

ACKNOWLEDGMENTS

We thank Brian Bonilla for excellent technical work with mosquitoes; Andre Laughinghouse, Kevin Lee, and Yonas Gebremicale for mosquito rearing; Van My Pham and Karina Sewell for excellent salivary gland dissections; and Glenn Nardone and Lisa Olano for MS/MS analysis. This research was supported by the Division of Intramural Research Program of the NIH/NIAID (AI001246, to E.C.) and by a subcontract from grant 1R01AI099483 (to Z.N.A.).

AUTHOR CONTRIBUTIONS

Conceptualization, E.C., Z.N.A., and I.M.-M.; methodology, I.M.-M., P.C.V.L., L.A., G.S., S. Brooks, A.E.W., and E.C.; investigation, I.M.-M., P.C.V.L., L.A., G.S., E.I., A.A., S. Brooks, B.B.K., A.E.W., and E.C.; writing – original draft, I.M.-M.; writing – review & editing, I.M.-M., L.A., E.I., S. Bolland, Z.N.A., and E.C.; funding acquisition, E.C. and Z.N.A.; resources, S. Bolland, H.A., Z.N.A., and E.C.

DECLARATION OF INTERESTS

The authors declare no competing interests.

INCLUSION AND DIVERSITY

One or more of the authors of this paper self-identifies as an underrepresented ethnic minority in science. One or more of the authors of this paper received support from a program designed to increase minority representation in science.

Received: November 17, 2021
Revised: February 1, 2022
Accepted: March 17, 2022
Published: April 12, 2022

REFERENCES

Andrade, B.B., Teixeira, C.R., Barral, A., and Barral-Netto, M. (2005). Haematophagous arthropod saliva and host defense system: a tale of tear and blood. Acad. Bras Cienc. *77*, 665–693.

Araki-Sasaki, K., Aizawa, S., Hiramoto, M., Nakamura, M., Iwase, O., Nakata, K., Sasaki, Y., Mano, T., Handa, H., and Tano, Y. (2000). Substance P-induced cadherin expression and its signal transduction in a cloned human corneal epithelial cell line. J. Cell Physiol. *182*, 189–195. https://doi.org/10.1002/(sici)1097-4652(200002)182:2.

Arca, B., and Ribeiro, J.M. (2018). Saliva of hematophagous insects: a multifaceted toolkit. Curr. Opin. Insect Sci. *29*, 102–109. https://doi.org/10.1016/j.cois.2018.07.012.

Assis, J.B., Cogliati, B., Esteves, E., Capurro, M.L., Fonseca, D.M., and Sá-Nunes, A. (2021). *Aedes aegypti* mosquito saliva ameliorates acetaminophen-induced liver injury in mice. PLoS One *16*, e0245788. https://doi.org/10.1371/journal.pone.0245788.

Basu, S., Aryan, A., Haac, M.E., Myles, K.M., and Adelman, Z.N. (2016). Methods for TALEN evaluation, use, and mutation detection in the mosquito *Aedes aegypti*. Methods Mol. Biol. *1338*, 157–177. https://doi.org/10.1007/978-1-4939-2932-0_13.

Basu, S., Aryan, A., Overcash, J.M., Samuel, G.H., Anderson, M.A., Dahlem, T.J., Myles, K.M., and Adelman, Z.N. (2015). Silencing of end-joining repair for efficient site-specific gene insertion after TALEN/CRISPR mutagenesis in *Aedes aegypti*. Proc. Natl. Acad. Sci. U S A. *112*, 4038–4043. https://doi.org/10.1073/pnas.1502370112.

Beerntsen, B.T., Champagne, D.E., Coleman, J.L., Campos, Y.A., and James, A.A. (1999). Characterization of the Sialokinin I gene encoding the salivary vasodilator of the yellow fever mosquito, *Aedes aegypti*. Insect Mol. Biol. *8*, 459–467.

Calvet, G., Aguiar, R.S., Melo, A.S.O., Sampaio, S.A., de Filippis, I., Fabri, A., Araujo, E.S.M., de Sequeira, P.C., de Mendonça, M.C.L., de Oliveira, L., et al. (2016). Detection and sequencing of Zika virus from amniotic fluid of fetuses with microcephaly in Brazil: a case study. Lancet Infect. Dis. *16*, 653–660.

Chagas, A.C., Calvo, E., Rios-Velasquez, C.M., Pessoa, F.A., Medeiros, J.F., and Ribeiro, J.M. (2013). A deep insight into the sialotranscriptome of the mosquito, *Psorophora albipes*. BMC Genomics *14*, 875. https://doi.org/10.1186/1471-2164-14-875.

Champagne, D.E., and Ribeiro, J.M. (1994). Sialokinin I and II: vasodilatory tachykinins from the yellow fever mosquito *Aedes aegypti*. Proc. Natl. Acad. Sci. U S A. *91*, 138–142.

Choi, J.E., and Di Nardo, A. (2018). Skin neurogenic inflammation. Semin. Immunopathol. *40*, 249–259. https://doi.org/10.1007/s00281-018-0675-z.

Galley, H.F., and Webster, N.R. (2004). Physiology of the endothelium. Br. J. Anaesth. *93*, 105–113. https://doi.org/10.1093/bja/aeh163.

Gentry, M.K., Henchal, E.A., McCown, J.M., Brandt, W.E., and Dalrymple, J.M. (1982). Identification of distinct antigenic determinants on dengue-2 virus using monoclonal antibodies. Am. J. Trop. Med. Hyg. *31*, 548–555. https://doi.org/10.4269/ajtmh.1982.31.548.

Giraldo-Calderon, G.I., Emrich, S.J., MacCallum, R.M., Maslen, G., Dialynas, E., Topalis, P., Ho, N., Gesing, S., Madey, G., Collins, F.H., and Lawson, D. (2015). VectorBase: an updated bioinformatics resource for invertebrate vectors and other organisms related with human diseases. Nucleic Acids Res. *43*, D707–D713. https://doi.org/10.1093/nar/gku1117.

Green, D.P., Limjunyawong, N., Gour, N., Pundir, P., and Dong, X. (2019). A mast-cell-specific receptor mediates neurogenic inflammation and pain. Neuron *101*, 412–420.e3. https://doi.org/10.1016/j.neuron.2019.01.012.

Griffith, O.W., and Kilbourn, R.G. (1996). Nitric oxide synthase inhibitors: amino acids. In Methods in Enzymology (Academic Press), pp. 375–392. https://doi.org/10.1016/S0076-6879(96)68040-9.

Guerrero, D., Cantaert, T., and Missé, D. (2020). *Aedes* mosquito salivary components and their effect on the immune response to arboviruses. Front. Cell Infect. Microbiol. *10*, 407. https://doi.org/10.3389/fcimb.2020.00407.

Hastings, A.K., Uraki, R., Gaitsch, H., Dhaliwal, K., Stanley, S., Sproch, H., Williamson, E., MacNeil, T., Marin-Lopez, A., Hwang, J., et al. (2019). *Aedes aegypti* NeSt1 protein enhances Zika virus pathogenesis by activating neutrophils. J. Virol. *93*. https://doi.org/10.1128/jvi.00395-19.

Heeman, W., Steenbergen, W., van Dam, G., and Boerma, E.C. (2019). Clinical applications of laser speckle contrast imaging: a review. J. Biomed. Opt. *24*, 080901. https://doi.org/10.1016/j.actatropica.2019.03.026.

Henrique, M.O., Neto, L.S., Assis, J.B., Barros, M.S., Capurro, M.L., Lepique, A.P., Fonseca, D.M., and Sa-Nunes, A. (2019). Evaluation of inflammatory skin infiltrate following *Aedes aegypti* bites in sensitized and non-sensitized mice reveals saliva-dependent and immune-dependent phenotypes. Immunol *158*, 47–59. https://doi.org/10.1111/imm.13096.

Hodo, T.W., de Aquino, M.T.P., Shimamoto, A., and Shanker, A. (2020). Critical neurotransmitters in the neuroimmune network. Front. Immunol. *11*, 1869. https://doi.org/10.3389/fimmu.2020.01869.

Iwanaga, S., Isawa, H., and Yuda, M. (2014). Horizontal gene transfer of a vertebrate vasodilatory hormone into ticks. Nat. Commun. *5*, 3373. https://doi.org/10.1038/ncomms4373.

Jiang, M.H., Chung, E., Chi, G.F., Ahn, W., Lim, J.E., Hong, H.S., Kim, D.W., Choi, H., Kim, J., and Son, Y. (2012). Substance P induces M2-type macrophages after spinal cord injury. Neuroreport *23*, 786–792. https://doi.org/10.1097/WNR.0b013e3283572206.

Kauffman, E.B., and Kramer, L.D. (2017). Zika virus mosquito vectors: competence, biology, and vector control. J. Inf. Dis. *216*, S976–S990. https://doi.org/10.1093/infdis/jix405.

Kern, O., Valenzuela Leon, P.C., Gittis, A.G., Bonilla, B., Cruz, P., Chagas, A.C., Ganesan, S., Ribeiro, J.M.C., Garboczi, D.N., Martin-Martin, I., and Calvo, E. (2021). The structures of two salivary proteins from the West Nile vector *Culex quinquefasciatus* reveal a beta-trefoil fold with putative sugar binding properties. Curr. Res. Struct. Biol. *3*, 95–105. https://doi.org/10.1016/j.crstbi.2021.03.001.

Ko, J.A., Murata, S., and Nishida, T. (2009a). Up-regulation of the tight-junction protein ZO-1 by substance P and IGF-1 in A431 cells. Cell Biochem. Funct. *27*, 388–394. https://doi.org/10.1002/cbf.1587.

Ko, J.A., Yanai, R., and Nishida, T. (2009b). Up-regulation of ZO-1 expression and barrier function in cultured human corneal epithelial cells by substance P. FEBS Lett. *583*, 2148–2153. https://doi.org/10.1016/j.febslet.2009.05.010.

Kojima, H., Sakurai, K., Kikuchi, K., Kawahara, S., Kirino, Y., Nagoshi, H., Hirata, Y., and Nagano, T. (1998). Development of a fluorescent indicator for nitric oxide based on the fluorescein chromophore. Chem. Pharm. Bull. *46*, 373–375. https://doi.org/10.1248/cpb.46.373.

Kojin, B.B., Tsujimoto, H., Jakes, E., O'Leary, S., and Adelman, Z.N. (2021). Indel Detection following CRISPR/Cas9 mutagenesis using high-resolution melt analysis in the mosquito *Aedes aegypti*. J. Vis. Exp. https://doi.org/10.3791/63008.

Kolhekar, A.S., Roberts, M.S., Jiang, N., Johnson, R.C., Mains, R.E., Eipper, B.A., and Taghert, P.H. (1997). Neuropeptide amidation in Drosophila: separate genes encode the two enzymes catalyzing amidation. J. Neurosci. *17*, 1363–1376. https://doi.org/10.1523/jneurosci.17-04-01363.1997.

Laurindo, F.R.M., Liberman, M., Fernandes, D.C., and Leite, P.F. (2018). Chapter 8 - endothelium-dependent vasodilation: nitric oxide and other mediators. In Endothelium and Cardiovascular Diseases, P.L. Da Luz, P. Libby, A.C.P. Chagas, and F.R.M. Laurindo, eds. (Academic Press), pp. 97–113. https://doi.org/10.1016/B978-0-12-812348-5.00008-8.

Lefteri, D.A., Bryden, S.R., Pingen, M., Terry, S., Beswick, E.F., Georgiev, G., Van der Laan, M., Mastrullo, V., Campagnolo, P., Waterhouse, R., et al. (2021). Mosquito saliva sialokinin-dependent enhancement of arbovirus infection through endothelial barrier leakage. Preprint at bioRxiv. https://doi.org/10.1101/2021.02.19.431961.

Lerner, E.A., Ribeiro, J.M., Nelson, R.J., and Lerner, M.R. (1991). Isolation of maxadilan, a potent vasodilatory peptide from the salivary glands of the sand fly *Lutzomyia longipalpis*. J. Biol. Chem. *266*, 11234–11236.

Lim, J.E., Chung, E., and Son, Y. (2017). A neuropeptide, Substance-P, directly induces tissue-repairing M2 like macrophages by activating the PI3K/Akt/mTOR pathway even in the presence of IFNγ. Sci. Rep. *7*, 9417. https://doi.org/10.1038/s41598-017-09639-7.

Mannangatti, P., Sundaramurthy, S., Ramamoorthy, S., and Jayanthi, L.D. (2017). Differential effects of aprepitant, a clinically used neurokinin-1 receptor antagonist on the expression of conditioned psychostimulant versus opioid reward. Psychopharmacol *234*, 695–705. https://doi.org/10.1007/s00213-016-4504-6.

Martin-Martin, I., Kern, O., Brooks, S., Smith, L.A., Valenzuela-Leon, P.C., Bonilla, B., Ackerman, H., and Calvo, E. (2020). Biochemical characterization of AeD7L2 and its physiological relevance in blood feeding in the dengue mosquito vector, *Aedes aegypti*. FEBS J. https://doi.org/10.1111/febs.15524.

Moncada, S., and Higgs, A. (1993). The L-arginine-nitric oxide pathway. N. Engl. J. Med. *329*, 2002–2012, PMID: 7504210. https://doi.org/10.1056/nejm199312303292706.

Montana, G., and Lampiasi, N. (2016). Substance P induces HO-1 expression in RAW 264.7 cells promoting switch towards M2-like macrophages. PLoS One *11*, e0167420. https://doi.org/10.1371/journal.pone.0167420.

Nguyen, L.S., Villablanca, A.C., and Rutledge, J.C. (1995). Substance P increases microvascular permeability via nitric oxide-mediated convective pathways. Am. J. Physiol. *268*, R1060–R1068. https://doi.org/10.1152/ajpregu.1995.268.4.R1060.

Page, N.M. (2013). Chapter 125 - tachykinins. In Handbook of Biologically Active Peptides, Second Edition, A.J. Kastin, ed. (Academic Press), pp. 943–950. https://doi.org/10.1016/B978-0-12-385095-9.00125-1.

Pingen, M., Bryden, S.R., Pondeville, E., Schnettler, E., Kohl, A., Merits, A., Fazakerley, J.K., Graham, G.J., and McKimmie, C.S. (2016). Host inflammatory response to mosquito bites enhances the severity of arbovirus infection. Immunity *44*, 1455–1469. https://doi.org/10.1016/j.immuni.2016.06.002.

Ribeiro, J.M. (1987). Role of saliva in blood-feeding by arthropods. Annu. Rev. Entomol. *32*, 463–478.

Ribeiro, J.M. (1992). Characterization of a vasodilator from the salivary glands of the yellow fever mosquito *Aedes aegypti*. J. Exp. Biol. *165*, 61–71.

Ribeiro, J.M. (2000). Blood-feeding in mosquitoes: probing time and salivary gland anti-haemostatic activities in representatives of three genera (*Aedes, Anopheles, Culex*). Med. Vet. Entomol. *14*, 142–148.

Ribeiro, J.M., Evans, P.M., MacSwain, J.L., and Sauer, J. (1992). *Amblyomma americanum*: characterization of salivary prostaglandins E2 and F2 alpha by RP-HPLC/bioassay and gas chromatography-mass spectrometry. Exp. Parasitol. *74*, 112–116. https://doi.org/10.1016/0014-4894(92)90145-z.

Ribeiro, J.M., Katz, O., Pannell, L.K., Waitumbi, J., and Warburg, A. (1999). Salivary glands of the sand fly *Phlebotomus papatasi* contain pharmacologically active amounts of adenosine and 5'-AMP. J. Exp. Biol. *202*, 1551–1559.

Ribeiro, J.M., Marinotti, O., and Gonzales, R. (1990). A salivary vasodilator in the blood-sucking bug, *Rhodnius prolixus*. Br. J. Pharmacol. *101*, 932–936. https://doi.org/10.1111/j.1476-5381.1990.tb14183.x.

Ribeiro, J.M., Martin-Martin, I., Arca, B., and Calvo, E. (2016). A deep insight into the sialome of male and female *Aedes aegypti* mosquitoes. PLoS One *11*, e0151400. https://doi.org/10.1371/journal.pone.0151400.

Ribeiro, J.M., and Modi, G. (2001). The salivary adenosine/AMP content of *Phlebotomus argentipes* Annandale and Brunetti, the main vector of human kala-azar. J. Parasitol. *87*, 915–917. https://doi.org/10.1645/0022-3395(2001)087[0915:TSAACO]2.0.CO;2.

Ribeiro, J.M., and Nussenzveig, R.H. (1993). The salivary catechol oxidase/peroxidase activities of the mosquito *Anopheles albimanus*. J. Exp. Biol. *179*, 273–287.

Ribeiro, J.M., Nussenzveig, R.H., and Tortorella, G. (1994). Salivary vasodilators of *Aedes triseriatus* and *Anopheles gambiae* (Diptera: Culicidae). J. Med. Entomol. *31*, 747–753. https://doi.org/10.1093/jmedent/31.5.747.

Ribeiro, J.M., Vachereau, A., Modi, G.B., and Tesh, R.B. (1989). A novel vasodilatory peptide from the salivary glands of the sand fly *Lutzomyia longipalpis*. Science *243*, 212–214.

Ribeiro, J.M.C., and Arca, B. (2009). From Sialomes to the Sialoverse: an insight into salivary potion of blood-feeding insects. Adv. Insect Phys. *37*, 59–118.

Ribeiro, J.M.C., Chagas, A.C., Pham, V.M., Lounibos, L.P., and Calvo, E. (2014). An insight into the sialome of the frog biting fly, *Corethrella appendiculata*. Insect Biochem. Mol. Biol. *44*, 23–32. https://doi.org/10.1016/j.ibmb.2013.10.006.

Ribeiro, J.M.C., Charlab, R., Pham, V.M., Garfield, M., and Valenzuela, J.G. (2004). An insight into the salivary transcriptome and proteome of the adult female mosquito *Culex pipiens quinquefasciatus*. Insect Biochem. Mol. Biol. *34*, 543–563. https://doi.org/10.1016/j.ibmb.2004.02.008.

Robinson, M.D., McCarthy, D.J., and Smyth, G.K. (2010). edgeR: a Bioconductor package for differential expression analysis of digital gene expression data. Bioinformatics *26*, 139–140. https://doi.org/10.1093/bioinformatics/btp616.

Schmid, M.A., Glasner, D.R., Shah, S., Michlmayr, D., Kramer, L.D., and Harris, E. (2016). Mosquito saliva increases endothelial permeability in the skin, immune cell migration, and dengue pathogenesis during antibody-dependent enhancement. PLoS Pathog. *12*, e1005676. https://doi.org/10.1371/journal.ppat.1005676.

Schneider, C.A., Rasband, W.S., and Eliceiri, K.W. (2012). NIH Image to ImageJ: 25 years of image analysis. Nat. Methods *9*, 671–675. https://doi.org/10.1038/nmeth.2089.

Seryogina, E., Mezentsev, M., Piavchenko, G., Dremin, V., Kozlov, I., Sdobnov, A., Stelmashchuk, O., Mamoshin, A., and Dunaev, A. (2019). Laser speckle contrast imaging of abdominal organs in mouse model. In Proc. SPIE 11065, Saratov Fall Meeting 2018: Optical and Nano-Technologies for Biology and Medicine, 110650Q (3 June 2019) (SPIE). https://doi.org/10.1117/12.2523185.

Severini, C., Improta, G., Falconieri-Erspamer, G., Salvadori, S., and Erspamer, V. (2002). The tachykinin peptide family. Pharmacol. Rev. *54*, 285–322. https://doi.org/10.1124/pr.54.2.285.

Song, H., Yin, W., Zeng, Q., Jia, H., Lin, L., Liu, X., Mu, L., and Wang, R. (2012). Hemokinins modulate endothelium function and promote angiogenesis through neurokinin-1 receptor. Int. J. Biochem. Cell Biol. *44*, 1410–1421. https://doi.org/10.1016/j.biocel.2012.04.014.

Souza-Neto, J.A., Powell, J.R., and Bonizzoni, M. (2019). *Aedes aegypti* vector competence studies: a review. Infect. Genet. Evol. *67*, 191–209. https://doi.org/10.1016/j.meegid.2018.11.009.

Steiner, D.F., Smeekens, S.P., Ohagi, S., and Chan, S.J. (1992). The new enzymology of precursor processing endoproteases. J. Biol. Chem. *267*, 23435–23438.

Sun, P., Nie, K., Zhu, Y., Liu, Y., Wu, P., Liu, Z., Du, S., Fan, H., Chen, C.-H., Zhang, R., et al. (2020). A mosquito salivary protein promotes flavivirus transmission by activation of autophagy. Nat. Commun. *11*, 260. https://doi.org/10.1038/s41467-019-14115-z.

Suvas, S. (2017). Role of Substance P Neuropeptide in inflammation, wound healing, and tissue homeostasis. J. Immunol. *199*, 1543–1552. https://doi.org/10.4049/jimmunol.1601751.

Tsujimoto, H., and Adelman, Z.N. (2021). Improved fecundity and fertility assay for *Aedes aegypti* using 24 well tissue culture plates (EAgaL Plates). JoVEe61232. https://doi.org/10.3791/61232.

Vogt, M.B., Lahon, A., Arya, R.P., Kneubehl, A.R., Spencer Clinton, J.L., Paust, S., and Rico-Hesse, R. (2018). Mosquito saliva alone has

profound effects on the human immune system. PLoS Negl. Trop. Dis. *12*, e0006439. https://doi.org/10.1371/journal.pntd.0006439.

Yang, L., Sui, W., Li, Y., Qi, X., Wang, Y., Zhou, Q., and Gao, H. (2016). Substance P inhibits hyperosmotic stress-induced apoptosis in corneal epithelial cells through the mechanism of Akt activation and Reactive Oxygen Species scavenging via the Neurokinin-1 Receptor. PLoS One *11*, e0149865. https://doi.org/10.1371/journal.pone.0149865.

Zeidner, N.S., Higgs, S., Happ, C.M., Beaty, B.J., and Miller, B.R. (1999). Mosquito feeding modulates Th1 and Th2 cytokines in flavivirus susceptible mice: an effect mimicked by injection of sialokinins, but not demonstrated in flavivirus resistant mice. Parasite Immunol. *21*, 35–44.

STAR★METHODS

KEY RESOURCES TABLE

REAGENT or RESOURCE	SOURCE	IDENTIFIER
Antibodies		
Rat anti-substance P monoclonal antibody	Millipore	Cat# MAB356, clone NC1; RRID: AB_94639
Goat anti-rat IgG-FITC antibody	Invitrogen	Cat# 31629; RRID: AB_228240
Purified rat anti-mouse CD16/CD32 (Mouse BD Fc Block™)	BD Biosciences	Cat# 553142; RRID: AB_394656
FITC anti-mouse CD64 (FcγRI) Antibody	BioLegend	Cat# 139316; RRID: AB_2566556, clone X54-5/7.1
PE anti-mouse CD170 (Siglec-F) Antibody	BD Biosciences	Cat# 552126; RRID: AB_394340, clone E50-2440
PerCP-Cy5.5 anti-mouse CD11c Antibody	BioLegend	Cat# 117326; RRID: AB_2129643, clone N418
PE/Cyanine7 anti-mouse Ly-6G Antibody	BioLegend	Cat# 127618; RRID: AB_1877261, clone 1A8
APC anti-mouse I-A/I-E Antibody (MHC-II)	BioLegend	Cat# 107614; RRID: AB_313329, clone M5/114.15.2
APC/Cyanine7 anti-mouse Ly-6C Antibody	BioLegend	Cat# 128026; RRID: AB_10640120, clone HK1.4
Brilliant Violet 421™ anti-mouse CD45.2 Antibody	BioLegend	Cat# 109832; RRID: AB_2565511, clone 104
PE anti-mouse/human CD11b Antibody	BioLegend	Cat# 101208; RRID: AB_312790, clone M1/70
FITC anti-mouse CD8a Antibody	BioLegend	Cat# 100706; RRID: AB_312745, clone 53-6.7
APC anti-mouse FcεRIα Antibody	BioLegend	Cat# 134316, RRID; AB_10640121, clone MAR-1
PerCP/Cyanine5.5 anti-mouse CD4 Antibody	BioLegend	Cat# 100540, RRID:; AB_893326, clone RM4-5
PE-Cy™7 rat anti-mouse CD19	BD Biosciences	Cat# 552854; RRID: AB_394495, clone 1D3
PerCP-Cy5.5 anti-mouse CD117 (c-Kit) Antibody	BioLegend	Cat# 105825; RRID: AB_1626278, clone 2B8
APC/Cyanine7 anti-mouse CD3 Antibody	BioLegend	Cat# 100222; RRID: AB_2057374, clone 17A2
FITC anti-mouse/human CD11b Antibody	BioLegend	Cat# 101206; RRID: AB_312789, clone M1/70
Mouse IgG antibody 4G2	Gentry et al. (1982) Provided by Dr. Steve Whitehead, NIAID, NIH.	N/A
Peroxidase-labeled goat anti-mouse IgG (used for virus titration)	SeraCare	Cat# 5450-0011; RRID: AB_2687537
Bacterial and virus strains		
2015 Fortaleza Zika virus strain	Calvet et al. (2016). Provided by Dr. Steve Whitehead, NIAID, NIH.	N/A
Biological samples		
Mouse third-order mesenteric arteries	This paper	N/A
Bovine whole blood in Acid Citrate Dextrose (ACD)	Lampire Biological Laboratories	Cat# 7200801
Chemicals, peptides, and recombinant proteins		
Pilocarpine hydrochloride	Sigma-Aldrich	Cat# P6503
Sialokinin I peptide: NH2-NTGDKFYGLM-Amide	Atlantic Peptides	N/A
Substance P peptide: NH2-RPKPQQFFGLM-Amide	Atlantic Peptides	N/A
4,5-Diaminofluorescein (DAF-2)	Cayman Chemical	Cat# 85160
L-NG-Nitro arginine methyl ester (L-NAME)	Sigma-Aldrich	Cat# N5751
Krebs-HEPES buffer	Boston BioProducts, Inc.	Cat # BSS-265
LC Green Plus+	Biofire Defense	Cat# BCHM-ASY-0005
Pfx polymerase	Thermo Fisher Scientific	Cat# 11708039
Paraformaldehyde	Fisher Scientific	Cat# 50-980-487
Bovine Serum Albumin	Sigma-Aldrich	Cat# A9576
Triton X-100	EMD Millipore, Fisher Scientific	Cat# M1122980101
Phalloidin Alexa Fluor 647 fluorophore	Thermo Fisher Scientific	Cat# A22287

(*Continued on next page*)

Continued

REAGENT or RESOURCE	SOURCE	IDENTIFIER
Vectashield with DAPI	Fisher Scientific	Cat# NC1695563
Aprepitant	Sigma-Aldrich	Cat# 170729-80-3
Dimethyl sulfoxide (DMSO)	Fisher Scientific	Cat# BP231-100
ATP	Sigma-Aldrich	Cat# 34369-07-8
Drabkin's reagent	Sigma-Aldrich	Cat# D5941
ACK lysis buffer	Lonza	Cat# 10548E
Minimum Essential Medium	Gibco, Thermo Fisher Scientific	Cat# 15188319
Sodium pyruvate	Gibco Thermo Fisher Scientific	Cat# 12539059
L-glutamine	Gibco, Thermo Fisher Scientific	Cat# 25030149
Non-essential amino acids	Gibco, Thermo Fisher Scientific	Cat# 11-140-050
Methylcellulose	Sigma-Aldrich	Cat# M0512
OptiMEM medium	Gibco, Thermo Fisher Scientific	Cat# 31985062
Penicillin–Streptomycin–Amphotericin B	Gibco, Thermo Fisher Scientific	Cat# 15240096
TrueBlue™ Peroxidase Substrate	Seracare	Cat# 5510-0030
RPMI 1640 media	Sigma-Aldrich	Cat# R8758
Phorbol-12-myristate-13-acetate (PMA)	Sigma-Aldrich	Cat# P8139
Nigericin	Sigma-Aldrich	Cat# N7143
Vascular Cell Basal Medium	ATCC	Cat# PCS-100-030
70-kDa FITC-dextran	Sigma-Aldrich	Cat# FD70S
Critical commercial assays		
DNA purification kit	Macherey-Nagel	Cat# 740609.50
MEGAscript™ T7 Transcription Kit	Thermo Fisher Scientific	Cat# AMB13345
MEGAclear™ Transcription Clean-Up Kit	Thermo Fisher Scientific	Cat# AM1908
Phire Animal Tissue Direct PCR Kit	Fisher Scientific	Cat# F140WH
Multi Tissue Dissociation kit -1	Miltenyi Biotec	Cat# 130-110-201
LIVE/DEAD™ Fixable Yellow Dead Cell Stain Kit	Thermo Fisher Scientific	Cat# L34959
Human ProcartaPlex mix & match 12-plex magnetic Luminex Assay kit	Thermo Fisher Scientific	Cat# PPX-12-MXTZ962
Caspase-Glo 1 Inflammasome Assay	Promega	Cat# G9951
Microvascular Endothelial Cell Growth Kit-BBE	ATCC	Cat# PCS-100-040
Deposited data		
Mass Spectrometry data from salivary glands of WT and KO mosquitoes	This paper	Table S1
Mass Spectrometry data from saliva of WT and KO mosquitoes	This paper	Table S2
Experimental models: Cell lines		
C6/36 cells	ATCC	Cat# CRL-1660
THP-1 cells	ATCC	Cat# TIB-202
Vero cells	ATCC	Cat# CCL-81
Human Primary Dermal Microvascular Endothelial Cells (HDMVECn)	ATCC	Cat# PCS-110-010
Experimental models: Organisms/strains		
Aedes aegypti Liverpool strain wild type	Virginia Tech, VA, USA	N/A
Aedes aegypti Liverpool strain sialoK^{i5} KO homozygous	This paper	N/A
Aedes aegypti Liverpool strain sialoK$^{\Delta 8}$ KO homozygous	This paper	N/A
C57BL/6NCrl mice	Charles River Laboratories	Cat# 027
BALB/cAnNCrl mice	Charles River Laboratories	Cat# 028

(*Continued on next page*)

Continued

REAGENT or RESOURCE	SOURCE	IDENTIFIER
Oligonucleotides		
Synthetic guide RNAs	This paper	See Table S3
SIAL-F: 5′-AGGATTTAATCTAACGTTGT-3′	Eurofins Genomics	N/A
SIAL-R: 5′-TGTAGCTGTTGGAAGAGAA-3′	Eurofins Genomics	N/A
Cas9 mRNA	Basu et al. (2015)	N/A
Software and algorithms		
Gen 5 software	Biotek Instruments	https://www.biotek.com/products/software-robotics-software/gen5-microplate-reader-and-imager-software/
GraphPad Prism v7	GraphPad Software	https://www.graphpad.com/
Lightscanner Call-IT 2.0 software	Basu et al. (2016) Kojin et al. (2021)	https://lightscanner.software.informer.com/2.0/
BioRender software	BioRender	https://biorender.com/
ImageJ software v1.52a	Schneider et al. (2012)	https://imagej.nih.gov/ij/
EdgeR	Kojin et al. (2021); Robinson et al. (2010)	https://bioconductor.org/packages/release/bioc/html/edgeR.html
Leica Application Suite X software	Leica Microsystems	https://www.leica-microsystems.com/products/microscope-software/p/leica-las-x-ls/
PIMSoft program v1.5	PeriMed	https://pimsoft.software.informer.com/1.5/
FlowJo software v10.6.1	TreeStar Technologies	https://www.flowjo.com/

RESOURCE AVAILABILITY

Lead contact

Further information and requests for resources and reagents should be directed to and will be fulfilled by the lead contact, Eric Calvo (ecalvo@niaid.nih.gov).

Materials availability

All unique/stable reagents generated in this study are available from the lead contact with a completed materials transfer agreement.

Data and code availability

Mass spectrometry raw data can be found in Tables S1 and S2. Any other data reported in this paper will be shared by the lead contact upon request.

No new custom code was generated for this paper.

Any additional information required to reanalyze the data reported in this paper is available from the lead contact upon request.

EXPERIMENTAL MODEL AND SUBJECT DETAILS

Animals

Eight-to 12-week old female C57BL/6NCrl (strain code 027) and BALB/cAnNCrl (strain code 028) mice were purchased from Charles River Laboratories (Wilmington, MA, USA). Purchasing company ensured that animals were free of the following pathogens: *Helicobacter*, MHV, MNV, MPV, and Parvovirus. Public Health Service Animal Welfare Assurance #A4149-01 guidelines were followed according to the National Institute of Allergy and Infectious Diseases (NIAID), National Institutes of Health (NIH) Animal Office of Animal Care and Use (OACU). These studies were carried out according to the NIAID-NIH animal study protocols (ASP) approved by the NIH Office of Animal Care and Use Committee (OACUC), with approval IDs ASP-LMVR3 and ASP-LMVR102. Animals were housed under SPF conditions with *ad libitum* access to food and water, and were randomly assigned to experimental groups. Experiments were performed using age- and sex-matched animals.

Cell lines

All cell lines described were cultured under temperature-controlled conditions at 37°C and 5% CO_2 with humidity. C6/36 cells derived from *Aedes albopictus* (ATCC®, Cat# CRL-1660) were grown in Minimum Essential Medium (MEM) pH 7.2, supplemented with 10% heat inactivated fetal bovine serum (FBS), sodium pyruvate, L-glutamine, and non-essential amino acids (all from Gibco at 1%). C6/36 cells were used for virus propagation. THP-1 cells (ATCC®, Cat# TIB-202) were grown in 10% FBS, RPMI 1640 media

(Sigma-Aldrich, St. Louis, MO). THP-1 cells were derived into macrophages for virus infection and immune responses studies. Vero cells (ATCC®, Cat# CCL-81) were grown in OptiPRO™ SFM (ThermoFisher) supplemented with 2 mM L-glutamine (Gibco). Vero cells were used for virus titration by plaque assay. Human Primary Dermal Microvascular Endothelial Cells (HDMVECn, ATCC®, Cat# PCS-110-010) were grown in Vascular Cell Basal Medium (ATCC®) supplemented with Microvascular Endothelial Cell Growth Kit-BBE (ATCC®) on 75 cm^2 culture flasks according to the manufacturer's instructions. HDMVECn were used for endothelial permeability assays. The cell lines have not been authenticated.

Virus

2015 Fortaleza Zika virus strain (Calvet et al., 2016) was provided by Dr. Steve Whitehead, NIAID, NIH, and propagated in C6/36 cells derived from *Ae. albopictus*.

METHOD DETAILS

Mosquito rearing, salivary gland dissection and saliva collection

Aedes aegypti (Liverpool strain, LVP) mosquitoes were reared in standard insectary conditions (27°C, 80% humidity with a 12-h light/dark cycle) at either the Department of Entomology and Fralin Life Science Institute, Virginia Tech or the Laboratory of Malaria and Vector Research, NIAID, NIH. Salivary glands from sugar-fed adult mosquitoes (5-7 days old) were dissected in PBS, pH 7.4 under a stereomicroscope. Salivary gland extract (SGE) was obtained by disrupting the gland walls by sonication (Branson Sonifier 450). Tubes were centrifuged at 12,000 × g for 5 min, and supernatants were kept at −80°C until used. Oil-induced saliva was collected as previously described with some modifications (Ribeiro, 1992). Briefly, alive mosquitoes were immobilized by placing their back on sticky tape. Mosquito mouthparts were inserted into 10 μl pipette tips containing mineral oil and salivation was promoted by injection of 200 nL of 3.6 mg/ml pilocarpine intrathoracically. One hour after salivation, pipette tips that contained oil with saliva droplets were combined in a tube with 10 μl of PBS, and the aqueous phase was separated by centrifugation.

Nitric oxide release of blood vessels

To investigate the molecular mechanism of action of sialokinin, we studied the nitric oxide release by blood vessels after incubation with sialokinin I or substance P as a control. DAF-2 (4,5-Diaminofluorescein; Cayman Chemical, cat. no. 85160) is a sensitive fluorescent indicator commonly used for the detection of nitric oxide (Kojima et al., 1998). In the presence of oxygen, it reacts with nitric oxide to yield the highly fluorescent triazolofluorescein (DAF-2T, Cayman Chemical), which can be detected by fluorescence.

Third-order mesenteric arteries (between 14 to 20 from each mouse) were isolated from the mesentery of eight-week-old C57/BL6 mice (Charles River Laboratories) that had been perfused of blood with Krebs-HEPES (KH) buffer (Boston BioProducts). After 30 min incubation with KH buffer at 37°C, tubes containing the arteries were briefly spun down to position arteries at the bottom of the tube; KH buffer was removed by pipetting and arteries were then incubated with 200 μl of KH buffer containing 5 μM DAF-2. After 10 min incubation, the correspondent buffer was removed and added to a black 96 flat bottom well plate (Corning) which served as the nitric oxide baseline. Then, arteries were incubated with 200 μl of KH buffer containing 100 μM of sialokinin I or substance P and 5 μM DAF-2. Lastly, to determine whether the nitric oxide release was caused by activation of nitric oxide synthase (NOS), L-NG-Nitro arginine methyl ester (L-NAME), an antagonist of NOS, was used. Arteries were incubated with L-NAME (Sigma) diluted to 10^{-4} M in 200 μl KH buffer for 40 min at 37 °C, which was later used as the baseline for each artery for L-NAME subsequent readouts. A pre-made solution of either 100 μM sialokinin I or 100 μM substance P in 200 μl of KH buffer containing 10^{-4} M L-NAME and 5 μM DAF-2 was added to the arteries. After 10 min incubation, supernatants were recovered and added to the 96 well plate. Fluorescence was determined at excitation and emission wavelengths of 485 and 538 nm, respectively, using a Cytation 5 reader (BioTek Instruments).

Unless indicated otherwise, all incubations were carried out at 37°C for 10 min in 200 μL of the correspondent buffer. A pilot experiment with 4 mice was developed to standardize the conditions. Experiments were carried out in biological duplicates. The effect of L-NAME was statistically analyzed using a paired t-test using GraphPad Prism v 7 (GraphPad Software). Images were created with BioRender.com.

Generation of CRISPR/Cas9 knockout lines

Cas9 mRNA and synthetic guide RNAs (sgRNAs) were synthesized and injected into *Ae. aegypti* embryos as described previously (Basu et al., 2015). Briefly, for each sgRNA (Table S3), a 60 nt-synthetic oligonucleotide containing a 20bp region of the *Ae. aegypti* sialokinin gene (AAEL000229: *sialokinin I*) was used in a PCR reaction with a common reverse strand oligonucleotide (5′-AAAAG CACCGACTCGGTGCCACTTTTTCAAGTTGATAACGGACTAGCCTTATTTTAACTTGCTATTTCTAGCTCTAAAAC-3′) using Pfx polymerase (Thermo-Fisher Scientific) according to the manufacturer's recommendations. Amplification conditions were 94°C, 10 s; 60°C for 30 s; 68°C for 15s and 34 cycles. Amplicons were purified (Machery-Nagel PCR purification kit) and used in an *in vitro* transcription reaction with MEGAscript T7 Transcription kit (Thermo Fisher Scientfic) to generate single-stranded guide RNAs; sgRNAs were further purified (MegaClear, Thermo-Fisher Scientific) and the concentrations determined. For embryo injections, a solution containing 600 ng/μl of Cas9 mRNA and 100 ng/μl of each sgRNA was injected into *Ae. aegypti* pre-blastoderm embryos as described (Basu et al., 2016). To detect editing activity, groups of ~100 embryos were sacrificed 24 h after injection, and genomic

DNA was extracted (Machery-Nagel DNA purification kit). PCR was performed in the presence of LC-Green dye using primers (SIAL-F, 5′-AGGATTTAATCTAACGTTGT-3′ and SIAL-R, 5′-TGTAGCTGTTGGAAGAGAA-3′). The resulting amplicon was melted using a LightScanner (Biofire, IdahoTechnologies), and differences in fluorescence determined (Kojin et al., 2021). To first validate sgRNA activity, three groups of ~100 embryos per injection set were used for genomic DNA extraction, followed by amplification of the *sialokinin* target region and melting curve analysis. Melting curve analysis is the quantitative analysis of the melt curves of product DNA fragments following PCR amplification. The use of DNA-binding dyes allows the identification of small variations in nucleic acid sequences and it is a good alternative for detection of mutants. For germline editing, injected embryos were allowed to hatch, and surviving adults (Generation 0, G_0) were mated in groups to individuals of the opposite sex from the parental strain. A subset of progeny (G_1) from these crosses were screened by leg PCR (Phire Animal Tissue Direct PCR Kit, Thermo Scientific) and HRMA as described previously (Basu et al., 2016). Amplicons with melting profiles distinct from the controls (parental strain) were purified as above and subjected to Sanger-based sequencing to identify any indels. To remove potential off-target edits and restore colony genetic diversity, individuals heterozygous for each mutation were crossed with WT mosquitoes, and heterozygous progeny selected for 4 additional generations before generating each stable homozygous line. At G_5, individuals heterozygous for each confirmed mutation in the *sialokinin I* gene were crossed to generate a homozygous loss-of-function mutant strain for each indel.

Mass spectrometry

Salivary gland extracts and saliva samples were submitted to mass spectrometry at Research and Technology Branch (NIAID, NIH). Salivary gland extracts were obtained from ten mosquitoes from each group, and two sets of saliva were collected from 50 mosquitoes each. Samples were reduced with 5 mM DTT for 40 min at 37°C, cooled to room temperature and alkylated with 15 mM iodoacetamide for 20 min. Then, extracts were hydrolyzed with 200 ng of GluC endoproteinase, a serine proteinase that preferentially cleaves peptide bonds C-terminal to glutamic acid residues and results in an improved sequence coverage in mass spectrometry, for 15 h at 37°C in 40 μl reactions buffered with 100 mM ammonium bicarbonate in the presence of 10% acetonitrile. The sample volumes were reduced under vacuum by ~50% at room temperature, and samples were acidified 0.5% trifluoroacetic acid and desalted/concentrated on Agilent OMIX10 C18 micro solid phase extraction tips. Samples were resuspended in 10 μl of 0.1% trifluoroacetic acid, 3% acetonitrile and submitted to nano LC-mass spectrometry (Thermo Fisher Orbitrap Fusion). For differential expression analysis, the number of unique mapping peptides was entered into EdgeR (Kojin et al., 2021; Robinson et al., 2010). p values were adjusted for multiple testing using the Benjamini–Hochberg method, with a final false discovery rate (FDR) set at 0.01.

Immunofluorescence

The presence of sialokinin peptides in the mosquito salivary glands was visualized by immunofluorescence as previously described by Ribeiro (Ribeiro, 1992) with several modifications. Briefly, salivary glands were dissected in PBS and fixed with 4% paraformaldehyde for 30 min. After three washes with PBS, samples were blocked with 1% bovine serum albumin, 0.5% Triton X-100, PBS (blocking solution) for 30 min. Salivary glands were incubated with a rat anti-substance P monoclonal antibody, specific for the carboxy terminal region of tachykinins (MAB356, clone NC1, Millipore), diluted 1:300 in blocking solution for 16 h at 4°C. We used salivary glands that were not incubated with anti-substance P antibody as a negative control. Moreover, another control to test the specificity of the reaction was included; a set of salivary glands from WT mosquitoes were incubated with anti-substance P monoclonal antibody pre-adsorbed with 0.1 mg/mL of substance P (Sigma) for 90 min at room temperature. Three 10-min washes with blocking solution were followed by the incubation with the goat anti-rat IgG-FITC antibody. Excess of secondary antibody was removed by another cycle of three 10 min washes. Samples were incubated with a Phalloidin Alexa Fluor 647 fluorophore (Fisher Scientific) diluted 1:50 in PBS for 20 min to stain actin in order to highlight the salivary gland wall architecture. After three additional washes, salivary glands were mounted on glass slides with Vectashield with DAPI. Bright field and fluorescent images were acquired in a Leica Epifluorescence Microscope, using a 20× objective with a 1× magnification. All incubations were performed in concavity slides at room temperature unless otherwise specified.

Peptide synthesis

Substance P (NH_2-RPKPQQFFGLM-Amide) and sialokinin I (NH_2-NTGDKFYGLM-Amide) were synthetized by Atlantic Peptides (Lewisburg, PA, USA). Synthetic peptides were amidated in the carboxy terminus to mimic all natural tachykinins, where the amide group is crucial for the biological activity (Severini et al., 2002). Lyophilized peptides were resuspended in water at 2 mg/mL and stored in 100 μL aliquots at −80°C.

Probing time

Probing time is the intradermal search for blood and is defined as the interval from the initial insertion of the mosquito mouthparts in the skin until visualization of first traces of blood in the midgut (Ribeiro, 2000). Adult female mosquitoes aged 5-10 days were deprived from sugar and water for 16 h. Mosquitoes were individually caged and offered either the back of a mouse or the breast of immobilized chicken. The backs of five-week-old C57BL/6 mice were shaved the day before the experiment. Mice were anesthetized (75 mg/kg of ketamine, 10 mg/kg of xylazine, i.p.) and kept on a slide warmer during mosquito exposure. Another set of mice were i.p. injected with 10 mg/kg of aprepitant (Sigma-Aldrich, St. Louis, MO, USA), a highly selective substance P receptor (NK1R) antagonist (Mannangatti et al., 2017). Aprepitant was dissolved in dimethyl sulfoxide (DMSO) and diluted with saline so

that the final DMSO concentration is 0.002% when injected. Mice were injected with aprepitant 15 min prior to anesthesia. For probing time experiments in chicken, animals were immobilized, and breast feathers removed. Probing time was also assessed on artificial membrane feeders (NDS Technologies, Inc, Vineland, NJ, United States) covered with Parafilm® M (Amcor, Ann Arbor, MI, USA) filled with bovine whole blood in Acid Citrate Dextrose (ACD) obtained from Lampire Biological Laboratories (Pipersville, PA, USA) supplemented with 2.4 mM ATP. Time was measured from the initial insertion of the mosquito mouthparts in the skin until visualization of first traces of blood in the midgut. All measurements were stopped at 300 s, and mosquitoes that showed a longer probing time were recorded as 300 s. Probing time experiments were performed blinded. Vials containing the mosquitoes were color coded according to mosquito group, and the color tape was covered with an extra layer of tape so the operators would not know which mosquito was being tested. After that measurement was taken, the color code was revealed. Two independent operators performed the probing time experiments. Overall, no differences were found between results from the two operators; therefore, results were combined and analyzed together. At least 60 mosquitoes were assayed per group. Results did not pass D'Agostino & Pearson normality test, so one-way ANOVA Kruskal-Wallis test was used to determine statistical power using GraphPad Prism v 7 (GraphPad Software). Images were created with BioRender.com.

Blood feeding success

Feeding time is the interval between the end of probing time and the instant a fully engorged mosquito pulls out the proboscis and flies away. Mosquito blood feeding success was evaluated on mice, chicken, and artificial blood meal through a membrane feeder. For each feeding experiment, cages each containing 100 female mosquitoes were starved from sugar and water the night before the experiment. C57BL/6 mice were anesthetized and placed on top of mosquito cages. Mosquitoes were allowed to feed on the animals or membrane feeders at 27°C for either 90 or 120 sec. One hour after blood feeding, mosquitoes were scored under a stereo microscope as fed if any traces of blood were visualized in their midgut, including partially fed and fully engorged status or unfed where no traces of blood were observed at all. For each experiment, two cages of mosquitoes were used for mosquito group and exposure time. Results from two different feeding success experiments were combined and analyzed together. Contingency analyses were performed by Chi-square and Fisher tests.

Differences in the amount of blood ingested by each mosquito were determined by quantification of total hemoglobin by using Drabkin's reagent (Sigma-Aldrich). Independently of the extended probing time in sialokinin-KO mosquitoes, we investigated if the process of imbibing blood was altered in the KO mosquitoes. The amount of blood ingested by individual mosquitoes was assessed at 90 and 120 sec of feeding time only in mosquitoes that had visual traces of blood in their midgut (partially and fully fed). Thirty blood-fed mosquitoes from each group (fully engorged and partially fed) were randomly selected and individually added to tubes that contained 2-4 disruption beads (Zirconia/Silica, 2.3 mm; Research Product International 9838, Mt. Prospect, USA). Mosquitoes were homogenized for 1 min at 4000 RPM in 1 ml of Drabkin's reagent using a Bullet Blender Storm (Next Advance, Troy, USA). Samples were cleared by centrifugation for 10 min at 13,000 x g at room temperature. Absorbance at 540 nm was read from three technical replicates from each biological sample (VersaMax microplate reader, Molecular Devices, San Jose, USA). Results were analyzed by one-way ANOVA using GraphPad Prism v 7 (GraphPad Software). Images were created with BioRender.com.

Fecundity and fertility assays

Sets of 24 blood fed mosquitoes for either 90 or 120 sec from the blood feeding success experiments on mouse, chicken and artificial blood meal were used. Mosquitoes were randomly picked from blood fed mosquitoes including fully and partially blood fed. 72 h post-blood feeding, fecundity and fertility experiments proceeded as described in (Tsujimoto and Adelman, 2021). Briefly, females were placed individually in a well in a 24-well plate of 10 mm diameter containing 1 mL of 2% agarose as a wet substrate for egg laying. They were allowed to lay eggs for 72 h and then released from the plate. Pictures of each well were taken, and eggs counted using ImageJ software (version 1.52a). Eggs were hatched with the addition of water on each well, and after 6-7 days post-eclosion, pictures of larvae were taken and counted the same way as the eggs. Results were analyzed by one-way ANOVA using GraphPad Prism v 7 (GraphPad Software). Images were created with BioRender.com.

In vivo blood perfusion by laser speckle imaging

To study differences in skin capillary blood flow during the bite of WT and sialokinin-KO mosquitoes, *in vivo* blood perfusion was assessed by laser speckle contrast analysis technology during mosquito blood feeding. Mouse hair was clipped from the region of interest (lower back) the day before the experiment. On the day of the experiment, sedated 12-week-old C57BL/6 mice were placed on a self-regulating temperature-control heading pad (PhysioSuite, Kent Scientific), set to maintain internal body temperature at 37.5 °C. Once sedation was achieved, the mouse was immediately placed under the blood perfusion camera (PeriCam PSI HR, PeriMed), 10 cm above the target tissue. Tissue blood perfusion was visualized in real time at a frame rate of 19 images/sec and a resolution of 0.02 mm. Mosquitoes that had been deprived from sugar for at least 16 h and whose wings had been clipped with fine scissors the day before the experiment were placed on the mouse hairless area. We introduced each mosquito into a popup mosquito rearing cage (BioQuip #1466AV) that contained the laser and the anesthetized mouse. To ensure mosquitoes began feeding at predictable times/locations, the wings of each mosquito were trimmed prior to the experiment, with mosquitoes deposited directly on top of the mouse area designated as the bite site. Wing-trimmed mosquitoes could walk but not fly away, and their feeding abilities were not

affected. To reduce confounding effects related to animal movement, we selected the lower back and hind leg area as the biting site, far from the diaphragm to minimize tissue movement from breathing. One mosquito at a time was placed on the clipped mouse area. Blood perfusion was measured for 1-2 min before the addition of the mosquito until 1-3 min after blood feeding. Results were expressed as the ratio of blood flow measured during/following exposure to the mosquito bite and the tissue at rest (baseline) in arbitrary perfusion units. Results based on the selected area of interest (mosquito bite) and times of interest (baseline, probing, feeding, 1- and 2-min post-feeding) were analyzed by PIMSoft program version 1.5 (PeriMed) using the baseline as the reference. Another region of interest outside the skin tissue was selected as a control. Ten independent measurements per mosquito group were taken. Laser speckle imaging studies were also performed after the injection of one salivary gland equivalent of SGE of WT or KO mosquitoes (2.3 μg) and PBS as a negative control in 10 μl using a 31-gauge needle. We measured the blood perfusion during and after injections of SGE and PBS as a control. Analysis was performed with readings at 2-min post-injection from 6 independent injections per group. Multiple comparisons were done by two-way ANOVA using GraphPad Prism v 7 (GraphPad Software).

In vivo cell recruitment to SGE injection or bites

Cell populations recruited to the skin were analyzed after either injection of salivary gland extracts (SGE) or bites of sialokinin-KO mosquitoes. For SGE injection, ten-week-old BALB/c mice were anesthetized with a mixture of ketamine and xylazine and animal footpads were injected intradermally/subcutaneously with 40 μL of sample using a 31G needle (EasyTouch). A total number of 16 mice were used. Samples were freshly prepared in PBS and filtered sterilized. The experimental mice footpads were injected with 6 μg of SGE from the different mosquito groups, and the same volume of PBS was used for control animals. For mosquito bite exposure, BALB/c mice were anesthetized with a mixture of ketamine and xylazine, as previously described, and their footpads exposed to mosquitoes that had been starved for one day. Sets of 10 mosquitoes were caged in 5 mL-Eppendorf vials, and each footpad was inserted in the vial through a fine mesh (Figure S4). Once the animals were sedated, we placed them on a self-regulating temperature-control heating pad (PhysioSuite, Kent Scientific) at 37°C on supine position and exposed their footpads to mosquitoes for 15 min. After exposure, mosquitoes were immediately crushed onto a tissue paper to confirm engorgement status and were scored as fed/unfed. A total number of 18 mice were used. After 24 h of SGE injection or mosquito bites, mice were euthanized, the footpads were removed and cut into pieces that were deposited in gentleMACS^{TM} C Tubes (Miltenyi Biotec) containing 2 ml of RPMI. To obtain a cell suspension, a mix of digesting enzymes (Multi Tissue Dissociation kit -1 Cat#130-110-201 Miltenyi Biotec) was added and incubated at 37°C for 45 min and homogenized using Multi tissue program from the gentleMACS^{TM} Dissociator (Miltenyi Biotec). After a short spin, homogenates were diluted in 5 mL of PBS and filtered using a 70 μm pore cell strainer (CellPro, Alkali Scientific). Cell suspensions were collected by centrifugation (3 min at 1200 rpm) and resuspended in 1 mL of ACK lysis buffer (Lonza) for 5 min at room temperature. Two mL of PBS supplemented with 5% FBS (ThermoFisher Scientific) were added, and cells were filtered again prior to centrifugation. Cell pellets were resuspended in PBS-FBS 5% with 1/500 dilution of Purified Rat Anti-Mouse CD16/CD32 (Mouse BD Fc Block^{TM}, BD, cat# 553142) to block non-specific binding. After 10 min of incubation at 4 °C, cells were distributed into tubes and stained with fluorescent-conjugated antibodies for surface markers for 30 min. The cytometry panels were chosen as previously described by Henrique et al. (2019). The following anti-mouse antibodies were used for the detection of leukocyte populations: CD64 (X54-5/7.1; FITC), SiglecF (E50-2440; PE), CD11c (N418; PerCP-Cy5.5), Ly6G (1A8; PE-Cy7), MHCII I-A/I-E (M5/114.15.2; APC), Ly6C (HK1.4; APC-Cy7), CD45.2 (104; BV421), CD11b (M1/70; PE, FITC), CD8 (53-6.7; FITC), FceRI (MAR-1; APC), CD4 (RM4-5; PerCP-Cy5.5), CD19 (1D3; PE-Cy7), cKit (2B8; PerCP-Cy5.5), CD3 (17A2; APC-Cy7). Live and dead cells were discriminated using LIVE/DEAD^{TM} Fixable Yellow Dead Cell Stain Kit (Fisher Scientific). Samples were acquired on a LSR II (BD Biosciences) or CytoFLEX (Beckman Coulter) flow cytometers and then analyzed with FlowJo v10.6.1 (TreeStar Technologies) software. Each footpad was analyzed independently.

Macrophage immune responses

Virus stock and virus titration

2015 Fortaleza Zika virus strain was propagated in C6/36 cells derived from *Aedes albopictus*. ZIKV stocks were prepared by infecting a monolayer of C6/36 cells for 48–72 h. Cells were cleared by centrifugation, the supernatant was concentrated to 1/10 of the starting volume using 100-kDa filter devices (Millipore sigma) and filtered through 0.22-μm membrane filters (Millipore sigma). The stock was aliquoted and stored at −80°C until further use.

Vero cells were seeded in 24-well plates until achieving 90% confluence; cells were infected with serial 10-fold dilutions of infected supernatants collected from THP-1 cells infected with ZIKV at 5 MOIs alone or ZIKV along with two pairs of SGE from SGE from sialoK^{i5}, sialoK$^{\Delta 8}$, or WT mosquitoes. Diluted samples were added to the Vero cells from which the culture medium was removed and incubated for 2 h at 32°C. After incubation, 1 mL of Overlay medium (1% methylcellulose (Sigma) with OptiMEM medium, 2% FBS, and 1% Penicillin–Streptomycin–Amphotericin B (all from Gibco)) was added to the wells. Plates were incubated for four days at 37°C, at 5% CO_2 and 90% humidity. After the overlay medium was discarded, plates were washed with 1X phosphate-buffered saline (1X PBS buffer) and fixed at room temperature for 30 min with 80% methanol and blocked with 5% PBS-milk for 20 min. Plates were washed and then incubated with mouse IgG antibody 4G2 (pan-flavivirus antibody provided by Dr. Steve Whitehead, NIAID, NIH) at 1:2000 dilution for 1 h. The primary antibody was removed, and plates were washed twice. Subsequently, Peroxidase-labeled goat anti-mouse IgG was added to the plates at a 1:2000 dilution and incubated for 1 h. Finally, plates were washed, and TrueBlue

Peroxidase substrate (KPL) was added to reveal the plaques. One-way ANOVA tests was used to determine statistical significance using GraphPad Prism v 7 (GraphPad Software).

Cytokines and inflammasome components determination in ZIKV infected macrophages

THP-1 cells (THP-1 (ATCC® TIB-202™) were grown in 10% FBS, RPMI 1640 media (Sigma-Aldrich, St. Louis, MO) and maintained at 37°C, 5% CO_2 in a humidified tissue culture incubator. THP-1 cells were counted and seeded at a concentration of 50,000 cells/well in 96 well plates in antibiotic-free 10% FBS, RPMI. Initially, THP-1 cells were treated with 50 ng/ml phorbol-12-myristate-13-acetate (PMA) (Sigma-Aldrich) in 10% FBS, RPMI media for 24 h to prime the THP-1 monocytes into macrophage-like cells followed by washing the PMA off and a 24 h rest period in fresh media prior to treatments. THP-1 cells were treated with ZIKV at 5 MOIs alone or ZIKV along with two pairs of SGE from sialoK^{i5}, sialoK$^{\Delta 8}$ or WT mosquitoes. As positive controls, cells were treated with Nigericin for 24 h. Supernatants of stimulated THP-1 macrophages were used for the measurement of the several cytokines. IL-6, IL-10, IFN gamma, IL-1β were analyzed using Human ProcartaPlex mix & match 12-plex magnetic Luminex Assay kit (PPX-12-MXTZ962) in a Luminex 200 instrument according to the manufacturer's instructions. The Caspase-1 activity was measured using the Caspase-Glo 1 Inflammasome Assay (Promega Co., Madison, WI, USA) according to the manufacturer's instructions. Briefly, 50 μL of supernatants from each well of stimulated THP-1 macrophage culture were transferred to the corresponding well of a new white 96-well plate. An aliquot of 50 μL of the Caspase-Glo 1 reagent was then added to each well and gently mixed on a plate shaker at 300 rpm for 30 s. The mixture was then incubated for 1h at room temperature before measuring the luminescence on a BioTek Cytation 5 reader (BioTek Instruments). One-way ANOVA tests was used to determine statistical significance using GraphPad Prism v 7 (GraphPad Software).

FITC-dextran endothelial permeability assay

Human Primary Dermal Microvascular Endothelial Cells (HDMVECn) were seeded on 1% gelatin-coated Transwell inserts (24-well, 0.4 mm, 6.5 mm insert; Corning Inc.) for a minimum of 4 days in the upper chamber, media was replaced with fresh medium every two days until we confirmed the cell monolayer integrity, by staining the cells with 1% of crystal violet. Thirty min before the assay, the medium of the lower chamber was replaced with basal medium supplemented with 3% FBS. After, filtered sterilized mosquito SGE (3.7 μg) was diluted with 1 mg/ml of 70-kDa FITC-dextran (Sigma) diluted in 3% FBS basal medium. The mixture was added to the upper chamber and incubated for 30 min at 37°C at 5% CO_2 and 90% humidity. Transwell inserts were removed, and 50 μL from each well were collected from duplicate wells and transferred to a black 96-well flat-bottom plate. The amount of FITC-dextran that migrated from the upper to the lower chamber was used as a proxy for cell permeability. FITC-dextran fluorescence was determined at excitation and emission wavelengths of 485 and 538 nm, respectively, using a Cytation 5 reader (BioTek Instruments). Contents of the lower chamber of untreated cell monolayers were used as the baseline control. One-way ANOVA tests was used to determine statistical significance using GraphPad Prism v 7 (GraphPad Software).

QUANTIFICATION AND STATISTICAL ANALYSIS

Statistics were calculated using GraphPad Prism v7 and are displayed as mean ± SEM or ±SD, as appropriate. N numbers indicate biological replicates. Data distribution was assessed by D'Agostino & Pearson normality test. Student's t-test or Kruskal-Wallis were used for pairwise comparisons, one- and two-way ANOVA for multiple group comparisons, as appropriate. For feeding success studies, contingency analyses were performed by Chi-square and Fisher tests. For differential expression analysis of mass spectrometry data, the number of unique mapping peptides was entered into EdgeR (Kojin et al., 2021; Robinson et al., 2010). p values were adjusted for multiple testing using the Benjamini–Hochberg method, with a final false discovery rate (FDR) set at 0.01. p values < 0.05 *, ≤ 0.01 **, ≤ 0.001 ***, ≤ 0.0001 ****. Detailed statistical information can be found in each section of the method details and figure legends.